

Tsunami hazard assessment along the north shore of Hispaniola from far- and near-field Atlantic sources

Stéphan T. Grilli¹ · Annette R. Grilli¹ · Eric David² ·
Christophe Coulet²

Received: 31 July 2015 / Accepted: 30 January 2016 / Published online: 17 February 2016
© Springer Science+Business Media Dordrecht 2016

Abstract Since the devastating earthquake of 2010 in Haiti, significant efforts have been devoted to estimating future seismic and tsunami hazard in Hispaniola. In 2013, following a workshop of experts, UNESCO commissioned an initial modeling study to assess tsunami hazard, essentially from seismic sources, along the North shore of Hispaniola (NSOH), which is shared by the Republic of Haiti (RH) and the Dominican Republic (DR). The scope of this study included detailed tsunami inundation mapping for two selected critical sites, Cap Haitien in RH and Puerto Plata in DR. Results of this effort are reported here, and, although still limited in scope, they are within the framework and contribute to the advancement of the UNESCO IOC Tsunami and other Coastal Hazards Warning System for the Caribbean and Adjacent Regions (CARIBE EWS; von Hillebrandt-Andrade in Science 341:966–968, 2013). In similar work done for critical areas of the US east coast (under the auspice of the US National Tsunami Hazard Mitigation Program), the authors have modeled the most extreme far-field tsunami sources in the Atlantic Ocean basin, including: (1) a hypothetical M_w 9 seismic event in the Puerto Rico Trench (PRT); (2) a repeat of the historical 1755 M_w 9 earthquake in the Azores convergence zone (LSB); and (3) a hypothetical extreme 450 km³ flank collapse of the Cumbre Vieja Volcano (CVV) in the Canary Archipelago. Here, tsunami hazard assessment is performed along the NSOH for these three sources, plus two additional near-field coseismic tsunami sources: (1) a M_w 8 earthquake in the western segments of the nearshore Septentrional fault (SF), as a repeat of the 1842 event; and (2) a M_w 8.7 earthquake occurring in selected segments of the North Hispaniola Thrust Fault (NHTF). Initial tsunami elevations are modeled based on each source's parameters and propagated with FUNWAVE-TVD (a nonlinear and dispersive long-wave Boussinesq model) in a series of increasingly fine-resolution nested grids (from 1 arc-min to 205 m) using a one-way coupling methodology. For the two selected sites, coastal inundation is computed with TELEMAC (a Nonlinear Shallow Water wave model),

✉ Stéphan T. Grilli
grilli@egr.uri.edu

¹ Department of Ocean Engineering, University of Rhode Island, Narragansett, RI, USA

² Artelia, Echirrolles, France

in finer-resolution (12–30 m) unstructured nested grids. While for the EC, PRT is a far-field source, for RH and DR, this would be local source as some of the NSOH would be affected within 1 h or is within 200 km of the PRT. This is per definitions of UNESCO IOC. Regional goes from 200 to 1000 km and within 1 and 3 h, and distant is greater than 3 h and more than 1000 km. We find that among the far-field sources CVV causes the largest impact, with up to 20-m runup at the critical sites while PRT, which is a local source for the NSOH, only causes up to 4-m runup due to its directionality; PRT, however, has both a much shorter return period and would impact the NSOH within 30 min of the earthquake. Among near-field sources, the SF event, as could be expected from a strike-slip fault, only causes a small tsunami, but the NHTF event causes up to 12-m runup in the critical sites, with the tsunami arriving within minutes of the earthquake. Hence, the latter event can be considered as the “Probable Maximum Tsunami” (PMT; following, e.g., the US Nuclear Regulatory Commission terminology) for the NSOH. Results of detailed coastal modeling for this PMT can be used to develop maps of vulnerability for the critical sites and prepare for mitigating measures and evacuation; a few examples of such maps are given in the paper. Although a number of earlier studies have dealt with each of the far-field tsunami sources, the modeling of their impact on the NSOH and that of the near-field sources, presented here as part of a comprehensive tsunami hazard assessment study, are novel. Future work should model additional coastal sites and may consider effects of tsunamis generated by near-field submarine mass failures.

Keywords Tsunami propagation · Coastal geohazard · Boussinesq wave models · Earthquakes

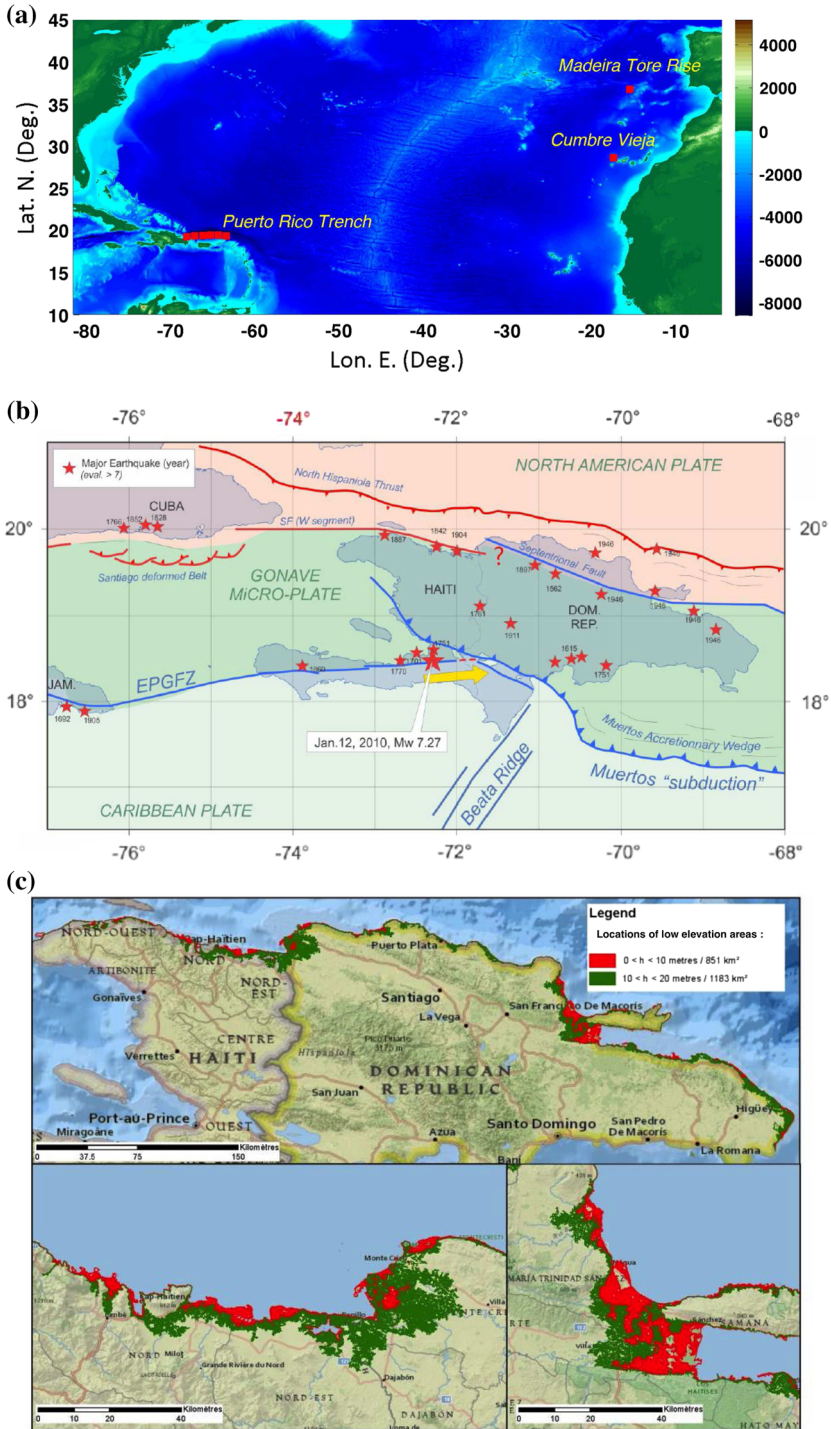
1 Introduction

On January 12, 2010, a devastating M_w 7 earthquake (Calais et al. 2010; Hayes et al. 2010) struck the Republic of Haiti (RH), causing over 230,000 fatalities, in great part because neither the authorities nor the population and infrastructures were prepared for such a major magnitude event. The earthquake also caused a small local tsunami (Fritz et al. 2013) that added to the destruction and casualties on Haiti’s west shore (Fig. 1). [Note that not only this tsunami was observed in the Baie de la Gonave (Hornbach et al. 2010), but a separate sourced tsunami was observed on the south coast of both the RH and the DR as well as at the tide gauge in Santo Domingo and the DART buoy in the Caribbean Sea (Fritz et al. 2013).] Since this catastrophic event, many efforts have been devoted to better characterizing seismic hazard in Hispaniola, in order to prepare for and mitigate the impact of future large events. Of particular concern was the tsunami hazard along the north shore of Hispaniola (NSOH) resulting from future large seismic events, both locally and regionally (Fig. 1c). The NSOH is skirted by two of the major faults of Hispaniola, the nearshore Septentrional fault (SF) (a strike-slip fault) and the North Hispaniola Thrust fault (NHTF) (a thrust fault), which runs parallel to it further north (Fig. 1b). These two faults mark the southern and northern boundaries, respectively, of the North Hispaniola micro-plate, north of the Gonave micro-plate (Benford et al. 2012). In 1842, Haiti’s north shore, and particularly the cities of Cap Haitien and Port-de-Paix, were struck by an earthquake with an estimated M_w 7.6–8.1 magnitude (Calais et al. 2010; UNESCO 2013); a tsunami was triggered. Both the earthquake and tsunami caused extensive destruction of Haiti’s

north shore and the area east of it, which nowadays constitutes the north shore of the Dominican Republic (DR); the earthquake caused 5000 fatalities, and the tsunami another 300 (see ten Brink et al. 2011; Gailler et al. 2015, for a historical perspective in the region as well as a more detailed report of the impact and discussion of the possible source of the 1842 event). Although somewhat questionable, some reports indicate that the 1842 tsunami caused significant runup in the far-field, particularly in the Lesser Antilles, with 0.9 m in Basse-Terre (Guadeloupe) and 1.8 m in Brequia Island (Grenadines) (Lander 1997).

In July 2013, a group of experts met in Port-au-Prince, as part of a workshop to assess: “Earthquake and tsunami hazard in Northern Haiti: Historical Events and Potential Sources”. They issued recommendations to serve as a basis for performing earthquake and tsunami hazard assessment and risk reduction projects in the area (UNESCO 2013). These discuss the source of the 1842 event (which may have been located in the SF or the NHTF, as put forth by Gailler et al. (2015) after this study was completed) and those of other relevant potential earthquakes and tsunamis that could impact Haiti’s north shore. In the near-field, several faults or fault segments were identified that could generate large potentially tsunamigenic earthquakes (Fig. 1b). Non-seismic sources of tsunamis in northern Haiti were also considered, e.g., submarine mass failures (SMFs), which it is believed may have played a role during the 1842 event. (In view that this event potentially took place in the SF, a strike-fault which as we shall see below is only weakly tsunamigenic, and generated a significant “localized” tsunami, in the authors’ opinion, there is strong evidence to consider additional sources such as SMFs.) The report concluded that “there is currently very limited information on the tsunami risk and potential tsunami sources in northern Haiti” and, for this reason, recommended that paleo-tsunami studies and more studies to refine parameters of potential fault and landslide sources be conducted. They also recommended to perform tsunami inundation studies and, based on the current incomplete knowledge of sources, that even a coarse or limited modeling study should be conducted to identify the areas most vulnerable to tsunami inundation that could be the object of tsunami evacuation in future events. Based on these recommendations, UNESCO commissioned a preliminary, but fairly comprehensive, tsunami hazard assessment study along the NSOH, from both near- and far-field (essentially seismic) sources. (It should be pointed out that this initial study did not include near-field SMFs.) The study was to be performed at the regional scale, at a fairly coarse resolution, but also locally in greater details and at a higher resolution for two selected critical sites, one in RH: Cap Haitien, and one in DR: Puerto Plata Fig. 1c). This paper reports on this initial effort.

Since 2010, under the auspice of the US National Tsunami Hazard Mitigation Program (NTHMP), the two lead authors and coworkers have performed tsunami modeling work to develop tsunami inundation maps for the most critical or vulnerable areas of the US east coast (USEC). This has led to selecting and modeling the most extreme far-field tsunami sources, both historical and hypothetical, in the Atlantic Ocean basin, without consideration for their return period or probability, leading to so-called Probable Maximum Tsunamis (PMTs; following, e.g., the US Nuclear Regulatory Commission terminology). These included: (1) *far-field seismic* sources (Fig. 1a): (1) a series of M_w 9 sources in the Azores convergence zone, representing possible sources of the 1755 Lisbon earthquake (LSB; Barkan et al. 2008; Grilli et al. 2015b), and (2) a M_w 9 source in the Puerto Rico Trench (PRT; e.g., Grilli et al. 2010, 2015b); (2) a *far-field extreme flank collapse* (450 km³ volume) of the Cumbre Vieja Volcano (CVV) on La Palma (Canary Islands, Fig. 1a; e.g., Abadie et al. 2012; Tehranirad et al. 2015); and (3) *near-field SMFs* on or near the USEC continental shelf break (e.g., Grilli et al. 2015a).



◀ **Fig. 1** Tsunami hazard assessment on the North Shore of Hispaniola (NSOH): **a** North Atlantic Ocean Basin with location of far-field tsunami sources, and footprint and ETOPO1 bathymetry (meter) of FUNWAVE-TVD 1 arc-min spherical grid G1a (Table 1); **b** Seismo-tectonic context of Hispaniola, with locations of major plates and faults (e.g., NHTF and SF) (from UNESCO 2013; source: B. Mercier de Lépinay) **c** Geography of RH, DR and the NSOH, with locations of vulnerable sites (coastal areas below 10-m elevation are marked in red and those between 10- and 20-m elevations are marked in green); Cap Haïtien (19.76 N, −72.20 E) and Puerto Plata (19.80 N, −70.6833 E) are the two selected sites that are finely modeled in this work

Table 1 Parameters of model grids used in FUNWAVE-TVD to compute the propagation of far-field (G1a,b, G2, G22a) and near-field (G22b,c) sources. “Res.” refers to the resolution of Spherical (S) or Cartesian (C) type grids and N_x and N_y indicate the number of grid cells in each direction. For the Cartesian grids, the distances in brackets are the grid extents in each direction

Grid/Type	SW Lat. (N°)	NE Lat. (N°)	SW Lon. (W°)	NE Lon. (W°)	Res.	N_x	N_y
G1a/S	10	45	82	5	1 min	4620	2100
G1b/S	10	45	82	50	1 min	1920	2100
G2/S	16	24.9667	79	64.0333	20 s	2695	1615
G22a/C	19.5 (0 km)	21.6 (227 km)	73.3 (0 km)	68.6667 (446 km)	205 m	2176	1108
G22b/C	18.9118 (0 km)	22.0009 (332 km)	74.4981 (0 km)	68.6135 (609 km)	205 m	2970	1620
G22c/C	18.9118 (0 km)	22.0009 (332 km)	75.4981 (0 km)	69.6135 (609 km)	205 m	2970	1620

Here, we perform tsunami hazard assessment on the NSOH by simulating tsunami generation and propagation from the LSB, PRT, and CVV sources and, based on recommendations of UNESCO (2013), from two additional relevant near-field seismic sources: (1) a M_w 8 earthquake in the western segments of the SF, as a potential repeat of the 1842 event; and (2) an hypothetical M_w 8.7 earthquake occurring in selected segments of the NHTF. As indicated, no near-field SMF sources were considered in this initial study, but could be the object of future work. Although a number of earlier papers have dealt in detail with each of the selected far-field tsunami sources (see list above), or have studied earthquake and potential tsunami hazard from some near-field seismic sources around Hispaniola (e.g., ten Brink et al. 2008, 2011; Calais and Mercier de Lépinay 1995; Calais et al. 2010; Gailler et al. 2015), to our knowledge, the comprehensive modeling of coastal tsunami hazard from a combination of these far- and near-field sources on the NSOH reported here is novel. Details of numerical models and methodology are given in the next section, followed by details of source selection/parametrization, and results of tsunami simulations.

2 Tsunami propagation and inundation modeling

2.1 Numerical models

Tsunami propagation from each source to the NSOH is modeled using the nonlinear and dispersive two-dimensional (2D) Boussinesq long-wave model (BM) FUNWAVE-TVD, in a series of nested grids of increasing resolution toward the coast, by way of a one-way

coupling method. FUNWAVE-TVD is a newer implementation of FUNWAVE (Wei et al. 1995), which is fully nonlinear in Cartesian grids (Shi et al. 2012) and weakly nonlinear in spherical grids (Kirby et al. 2013). The model was efficiently parallelized for use on a shared memory cluster (over 90 % scalability is typically achieved), which allows using large grids at a reasonable computational cost. FUNWAVE has been widely used to simulate tsunami case studies (e.g., Day et al. 2005; Grilli et al. 2007, 2010, 2013c, 2015a, b; Ioualalen et al. 2007; Tappin et al. 2008, 2014; Abadie et al. 2012; Tehranirad et al. 2015). The two lead authors and coworkers have used this model and related methodology as part of tsunami inundation mapping along the USEC, performed for NTHMP, as mentioned above (e.g., Abadie et al. 2012; Grilli and Grilli 2013a, b; Grilli et al. 2015a, b; Tehranirad et al. 2015), and also for several other tsunami hazard assessment studies of coastal nuclear power plants in the USA (see <http://chinacat.coastal.udel.edu/nthmp.html>). Both spherical and Cartesian versions of FUNWAVE-TVD were validated through benchmarking and approved for NTHMP work (Tehranirad et al. 2011).

As they include frequency dispersion effects, BMs simulate more complete physics than models based on Nonlinear Shallow Water Equations (NSWE), which until recently were traditionally used to simulate coseismic tsunami propagation. Modeling frequency dispersion effects is important for accurately simulating landslide (SMF) tsunamis, which usually are made of shorter and hence more dispersive waves than for coseismic tsunamis (Watts et al. 2003). However, including dispersion is also important for accurately modeling the nearshore propagation and coastal impact of all types of tsunamis. This is because dispersive shock waves (a.k.a. undular bores) may appear near the crest of incoming long waves in increasingly shallow water (Madsen et al. 2008). The importance of dispersion in modeling tsunami propagation was confirmed by running FUNWAVE in both BM and NSWE modes, by Tappin et al. (2008) for the 1998 Papua New Guinea landslide tsunami, and by Ioualalen et al. (2007) for the 2004 Indian Ocean and Kirby et al. (2013) for the 2011 Tohoku, coseismic tsunamis. (See also Glimsdal et al. (2013) for a recent discussion of dispersive effects in tsunami propagation.)

The initial tsunami elevation of both far- and near-field seismic sources (LSB, PRT, SF, NHTF) that is used to initialize FUNWAVE-TVD is obtained from Okada's (1985) method, based on fault (or sub-fault) plane parameters (see details later). This method computes the seafloor deformation caused by a dislocation in a fault plane embedded in a homogeneous semi-infinite half-space. Assuming that water is incompressible and raise time is small, seafloor deformation is used as initial tsunami elevation on the free surface (without initial velocity) and defines what one refers to as the "seismic tsunami source".

Tsunami generation by a series of scenarios of subaerial slides triggered by a CVV flank collapse was simulated by Abadie et al. (2012), using a multi-material three-dimensional (3D) Navier-Stokes (NS) model, in which the slide was represented as a dense Newtonian fluid (Abadie et al. 2010). Here, following the same approach as reported in Tehranirad et al. (2015) to compute the CVV far-field impact on the USEC, we use results of Abadie et al.'s simulations with the 3D-NS model (THETIS), of the most extreme collapse scenario (with a 450 km³ volume; discussed below), to initialize FUNWAVE-TVD, as a surface elevation and depth-averaged current computed after tsunami generation has fully occurred (here after 20 min).

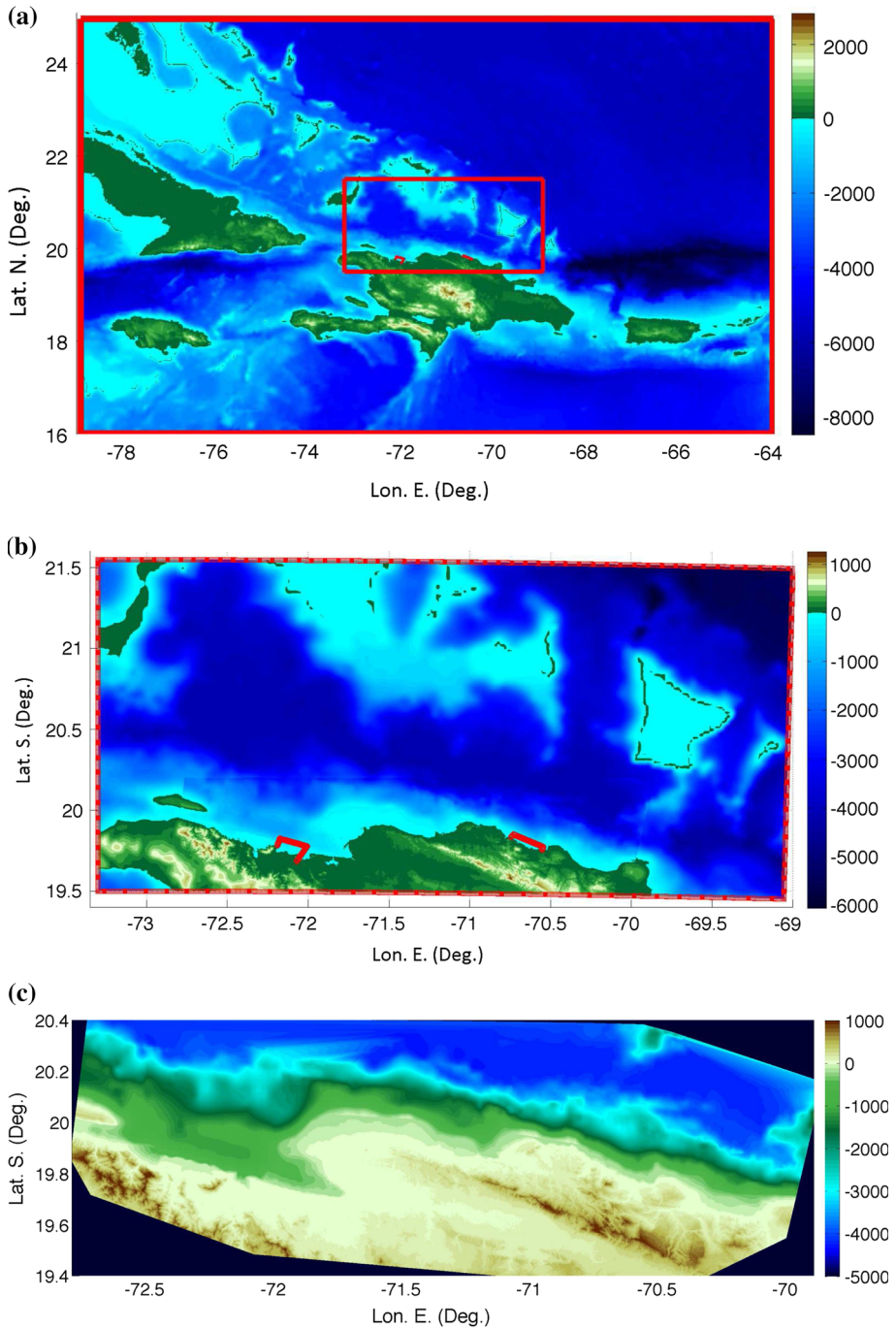
In deep water, coseismic tsunamis can be approximated by linear (non-dispersive) long waves. As they propagate into shallower water, however, they transform into more complex increasingly nonlinear wave trains, which may also feature dispersive undular bores (Madsen et al. 2008; Grilli et al. 2015a). Higher-frequency waves in such complex wave

trains end up breaking near- and onshore, similar to long ocean swell, while being transported by longer tsunami waves that cause the brunt of the inundation. FUNWAVE-TVD features the relevant physics to accurately simulate such processes, given enough grid resolution, and the model's computational efficiency allows simulating the entire propagation and coastal impact including dispersion; hence, if the physics calls for it, which is problem dependent, dispersion will express itself through the model equations. Additionally, dissipative processes from bottom friction and breaking waves are adequately represented in the model. Bottom friction is modeled as a quadratic term with a constant friction coefficient; in the absence of more specific data, we used the standard value $C_d = 0.0025$ of the bottom drag coefficient, which corresponds to coarse sand and is conservative as far as tsunami runup and inundation. Earlier work indicates that tsunami propagation results are not very sensitive to friction coefficient values in deeper water, but are more sensitive in shallow water, particularly when there is a wide shelf (Geist et al. 2009; Tehranirad et al. 2015; Grilli et al. 2015a), which is not the case for the NSOH. Additionally, Tehranirad et al. (2015) recently validated the dissipation of tsunami waves by bottom friction over shallow shelves, by comparing FUNWAVE-TVD results to an analytical solution. Breaking waves are captured using a front tracking (TVD) algorithm and switching to NSWs in grid cells where breaking has been detected (based on a breaking criterion). Earlier work shows that numerical dissipation in NSW models closely approximates the physical dissipation in breaking waves (Shi et al. 2012). Along the shore, FUNWAVE-TVD uses a moving shoreline algorithm that identifies wet and dry grid cells.

For computing onshore inundation, once incident tsunami waves have arrived nearshore in the form of trains of long waves and/or bores, dispersion no longer matters for wave evolution. Hence, onshore inundation can be accurately computed using a non-dispersive long-wave model, such as based on NSWs. In the present work, detailed onshore inundation in Cap Haiti and Puerto Plata is computed in high-resolution grids using the model TELEMAC-2D (<http://www.opentelemac.org/>), which solves NSWs on an unstructured triangular grid (12–30-m-size range). TELEMAC is forced by FUNWAVE-TVD results along an offshore boundary (Fig. 2b), in the form of time series of surface elevation and horizontal current. Inundation maps are prepared based on results of these simulations, together with other measures of tsunami coastal impact and related vulnerability. Only limited results of this phase of the work, however, are reported here, and details will be left out for a future publication dedicated to the vulnerability of the NSOH.

2.2 Methodology

Simulations of tsunami propagation with FUNWAVE-TVD are performed in nested grids, using a one-way coupling method (Fig. 2), in which time series of surface elevation and depth-averaged current are computed for a large number of stations/numerical wave gages, defined in a coarser grid, along the boundary of the finer grid used in the next level of nesting. Computations are fully performed in each coarser grid and then are restarted in the next level of finer grid, using the station time series as boundary conditions. As these include both incident and reflected waves computed in the coarser grid, this method closely approximates open boundary conditions. It was found in NTHMP work that a nesting ratio with a factor 3–4 reduction in mesh size allowed achieving good accuracy in tsunami simulations. Note that to prevent reflection in the first grid level, sponge layers are used along all the offshore boundaries (see details in Shi et al. 2012).



For regional inundation mapping caused by the far-field sources LSB and CVV, simulations are initiated in the ocean basin scale spherical grid G1a, which has a 1 arc-min resolution (about 1800 m) and covers the footprint of Fig. 1a (with 100–200-km-wide

Fig. 2 Tsunami hazard assessment on the North Shore of Hispaniola (NSOH). Footprint and topography of FUNWAVE-TVD's grids (Table 1): **a** 20 arc-sec spherical grid G2 (red box marks boundary of grid G22a) used for far-field source modeling; **b** 205-m Cartesian grid G22a (red boxes mark offshore boundaries of irregular (12–30-m resolution) grids used with TELEMAC, in Cap Haiti and Puerto Plata); and **c** Digitized 30-m bathymetry from maritime charts and land maps. Red dots in **a**, **b** mark locations of stations in the one-way-coupling method used with FUNWAVE-TVD (because of their high density, they appear as thick red lines in the figures). Color scale is bathymetry (meter), from 1 arc-min ETOPO-1 data and 30-m nearshore DEM

sponge layers along the open boundaries). Each of these far-field/local tsunami source is specified as initial conditions in the grid. For PRT, which is a local source with respect to the NSOH and is more north-south directional, a narrower version of the 1-min grid, referred to as G1b, is in fact used (Table 1). The second level of nesting for all three sources is the regional 20 arc-sec resolution grid G2 (about 500–600 m; Fig. 2a; Table 1), which is followed by a third-level Cartesian grid G22a, with a 205-m resolution (Fig. 2b; Table 1). For the 2 near-field tsunami sources, simulations are directly started in the 205-m resolution Cartesian grids G22b,c (using 20–50-km-wide sponge layers along the open boundaries; Table 1). The initial surface elevation and velocity (whether zero or not) of each tsunami source are specified in FUNWAVE-TVD's first grid level.

For each grid level, whenever possible, bathymetry and topography are interpolated from data of accuracy commensurate with the grid resolution (note, no smoothing of the bathymetry is done besides this interpolation). In deeper water, we use NOAA's 1 arc-min resolution ETOPO-1 data (Figs. 1a, 2a). In shallower water and on continental shelves, since no finer-resolution Digital Elevation Maps (DEMs) were publicly available along the NSOH (as, e.g., in the US, NOAA's NGDC 3" and 1" Coastal Relief Model data), we created a 30-m resolution DEM by digitizing maritime charts and land maps (Fig. 2c).

3 Results

3.1 Source parameters, tsunami generation, and initial propagation

In this section, we report on results of the parametrization, initialization, and initial propagation in FUNWAVE-TVD's of the: (1) 3 far-field sources (LSB, PRT and CVV) in the 1 arc-min grids G1a,b (Fig. 1a); as indicated above, PRT should and will more accurately be referred to as a local source, under the accepted UNESCO/IOC terminology, since as we shall see, it would impact the NSOH in under 1 h; (2) 2 near-field seismic sources (NHTF and SF) in the regional grids G22b,c (Fig. 2).

For the seismic sources, the required parameters of Okada's (1985) method include a fault plane area (width W and length L), depth at the source centroid, centroid location (lat-lon), 3 angles for orientation of the fault plane and slip vector (dip, strike, rake), and the shear modulus (μ) of the medium (10–60 Gpa, for shallow rupture in soft/poorly consolidated marine sediment to deep rupture in basalt). (Note the Poisson ratio of the medium is assumed to be 0.25 by default.) The moment magnitude of the anticipated earthquake is defined as, M_o (Nm) = μLWS , where S denotes fault slip. Thus, besides geometrical and material parameters, to complete the source parameterization, one needs either the slip or the M_o value of the considered event (or its magnitude, $M_w = (\log M_o)/1.5 - 6$, on a base 32 logarithmic scale, in MKS units). ten Brink et al. (2008) provide many parameters for tele-seismic sources and some of the regional sources in the North Atlantic. For the LSB

M_w 9 source, parameters were selected based on this and other studies of the 1755 event (see details later).

The PRT is a deep subduction zone (SZ) with a 600-km linear part orientated nearly E–W north of Puerto Rico (PR; dark blue area in Fig. 1a) that has a 20 month/year subduction rate (but in a fairly oblique direction). For a SZ, the magnitude for an extreme earthquake can be estimated by assuming a return period from an analysis of historical events and calculating the potential slip based on the SZ convergence rate. For the PRT seismic tsunami source to use in the NSOH study, UNESCO (2013) recommended to consider FEMA’s M_w 8.5 “catastrophic scenario for Puerto Rico”, which corresponds to an earthquake occurring on the 249-km part of the PRT located east of the western side of PR (from 64.5 to 67.1 Long. W), with a 5.47-m slip; this translates into a 270-year return period or so using the maximum subduction rate. While this may represent a catastrophic scenario for Puerto Rico, this is certainly not the most extreme one and also because it strikes the eastern side of the PRT, it is not the worst-case scenario for the NSOH either. Another way of designing the maximum earthquake expected in the PRT is to consider historical events both locally and in other similar SZs. Knight (2006) followed this approach and developed an estimate of the most extreme earthquake that could occur in the PRT to perform tsunami hazard assessment in the Caribbean region. He used a simple homogenous source covering the entire 600-km E–W length of the PRT by a 150-km width (three times the actual width of the seafloor trench), with a fault plane orientated based on local geology. He assumed an extreme source of magnitude M_w 9.0, leading to an average slip of 12 m (with $\mu = 3.3 \times 10^{10}$ GPa); based on the average PRT subduction rate, this slip yields an approximate 600-year return period. Grilli et al. (2010) performed a more detailed analysis of the PRT coseismic sources and tsunami generation, to estimate tsunami hazard on the north shore of Puerto Rico and along the USEC. They used Knight’s scenario as their extreme event, but also considered a smaller event over the same area of the SZ, with a M_w 8.7, corresponding to a 3.8-m slip and a 200-year or so return period. Note that the 200- and 600-year values are only orders of magnitude, assuming there is a periodicity of events of a certain magnitude in the region, which is far from being general and/or generally accepted (e.g., Corral 2006). A more rigorous analysis of earthquake and tsunami return periods would require a large data set of historical events, which is lacking for PRT. Grilli et al. (2010) noted that only one historical earthquake originated in the PRT, the 1787 M_w 8.1 event (with no information on tsunami generation); no large earthquake has occurred in the PRT since then. Here, with the aim of estimating tsunami hazard along the NSOH for the most extreme events (the so-called PMTs), we will consider the extreme M_w 9 PRT seismic source studied earlier; however, following more recent NTHMP work (Grilli et al. 2015b), we will more accurately account for the local geology of the PRT SZ by considering 12 sub-fault planes to define the source (see details later). It should be pointed out that should a smaller earthquake with similar slip strike a smaller area on the western side of the PRT (for instance, a M_w 8.5 earthquake with a 12-m slip striking a 240-km-long by 60-km-wide section of the PRT, of length similar to that of the FEMA scenario on the eastern side) it would create tsunami waves of similar height as those of the M_w 9 striking the entire SZ. Because of the E–W orientation of the PRT, these waves would have a similar impact on the NSOH as those of the larger M_w 9 earthquake considered here. Finally, with the lessons learned from the catastrophic Tohoku 2011 tsunami, which was caused by a M_w 9 earthquake that struck a 500 by 200 km area of the Japan Trench where the largest expected magnitude was M_w 8.5, causing nearly 20,000 fatalities and widespread destruction (Grilli et al. 2013c), we believe that it is wiser to be conservative and be prepared for the worst-case scenario.

For the two onshore and offshore near-field faults north of Hispaniola, approximate convergence/motion rates have been estimated from GPS measurements (Calais et al. 2010; Benford et al. 2012), yielding 9.8 ± 2.0 mm/year of motion along the SF and (based on Benford et al. 2012, Fig. 5) 2–6 mm/year of relative motion along the NHTF subduction zone. However, in each case, one also has to rely on other estimates such as historical seismic records (see Gailler et al. 2015 for details). Based on a consensus during the expert meeting, UNESCO (2013) identified 3 near-field earthquakes scenarios and provided fault plane parameters and expected maximum magnitudes for those. Here, we model UNESCO's scenario 1, which is intended to represent a possible source for the 1842 earthquake on the western side of the SF (2 segments), with a magnitude M_w 8.0, and UNESCO's scenario 3, which is intended to represent a worst-case near-field seismic scenario, with a magnitude M_w 8.7 on the entire length of the NHTF (3 segments). We do not simulate UNESCO's scenario 2, which is similar in magnitude to the 1946 event, but west of its actual epicenter, because it corresponds to a smaller magnitude M_w 8.1 event on the middle segment of scenario 3, with a smaller slip that will not cause a larger tsunami impact on the NSOH than scenario 3. These scenarios were also supported by other works, such as ten Brink et al. 2008; Calais et al. 2010, and Harbitz et al. 2012. With the fault slip provided by UNESCO (2013) for the 2 selected near-field sources, 10 and 5 m, respectively (parameters are detailed later; Tables 3 and 4), one could estimate return periods on the order of 2,500 and 500 years, respectively, for each event, based on the average plate motions listed above.

While the authors have modeled the LSB and PRT seismic sources as part of earlier NTHMP work (Grilli et al. 2010, 2015b; Grilli and Grilli 2013a, b), some source parameters were adjusted within the geophysical uncertainty, to maximize tsunami impact on the NSOH; additionally, both regional and local grids are different from those used in the earlier NTHMP work. Similarly, for near-field seismic sources, starting from the recommended values in the literature, some parameters will be selected within the geophysical uncertainty in order to maximize tsunami generation and impact on the NSOH, and particularly at the two selected critical sites of Cap Haiti and Puerto Plata.

Regarding the only non-seismic source considered here, the CVV flank collapse, while many geologists remain convinced that the extreme 450 km^3 scenario initially proposed by Ward and Day (2001) is still the most plausible, in view of both geologic evidence of past collapses and recent field work at CVV (S. Day, personal communication, 2015), the likelihood for such a large-scale event to occur at once is still controversial. For instance, the mechanism by which large volcanic debris avalanches occur (e.g., en masse or in successive stages) plays a key role on wave features and total energy; by analyzing turbidites in the Canary Islands, Wynn and Masson (2003) concluded that for some volcanos debris avalanches may have occurred in a retrogressive way, which obviously would have reduced their tsunamigenic potential. In contrast, McMurtry et al. (2007) hypothesized that ancient marine sediment deposits found in Bermuda Island were possibly related to a large tsunami caused by a giant Canarian landslide, of about the same age as the last CVV collapse (about 250ka). Adding to the evidence for megatsunamis triggered by extreme volcanic flank collapses, in a recent study of the Fogo volcano on the Cape Verde island, Ramalho et al. (2015) showed that a flank collapse may have catastrophically happened 73ka ago, as at least one fast voluminous event that triggered tsunamis of enormous height and energy, causing over 270-m runup on the nearby Santiago island. Because of the controversy surrounding the most extreme 450 km^3 scenario, Abadie et al. (2012) also simulated a 80 km^3 scenario, referred to as the CVV “expected extreme collapse”, that

was based on slope stability analyses of the CVV western flank. This scenario led to about one-third the coastal impact caused on the USEC by the most extreme scenario (Tehrani-rad et al. 2015). Here, after discussion with UNESCO during the course of the study, it was decided to be conservative and select for modeling the 450 km³ CVV scenario, keeping in mind that a multi-stage and/or a smaller volume collapse would significantly reduce the impact predicted on the NSOH. For this scenario, similar to Tehrani-rad et al.'s (2015) work, FUNWAVE-TVD will be initialized based on surface elevation and velocity computed at 20 min after the start of the event by Abadie et al. (2012).

Details of parameterization, tsunami generation, and initial oceanic propagation for each source are given in the following.

3.1.1 Far-field LSB seismic source

Although the exact location and parameters of the 1755 LSB event (Fig. 1), which is the basis for the far-field M_w 9 seismic source considered here, have been the object of intense research (e.g., Baptista et al. 1998a, b, 2003), they are still largely unknown. As part of the NTHMP-USEC work, Grilli and Grilli (2013a) modeled a dozen different sources of this magnitude, sited at various locations in the Açores convergence zone, with parameters selected based on Barkan et al.'s (2009) work. Strike angle, in particular, which strongly affects the tsunami directionality, was varied to cause maximum impact on various sections of the USEC. Here, we selected the location and strike angle that caused maximum impact in the Caribbean and Hispaniola (shown in Fig. 3a, b). The parameters of the fault plane are (Barkan et al. 2009): (1) fault plane center: -10.753 E Lon. 36.042 N Lat., (2) $L = 317$ km, (3) $W = 126$ km, (4) dip angle: 40° , (5) rake angle: 90° , (6) strike angle: 345° ; (7) slip $S = 20$ m, and (8) $\mu = 40$ GPa, which yields $M_o = 3.162 \times 10^{22}$ N m or $M_w = 9$. Using these parameters in Okada's model, we find the initial surface elevation shown in Fig. 3b. (Note that the CARIBE WAVE 2014 exercise organized under UNESCO (IOC 2013) used very similar fault parameters, although for a smaller M_w 8.5 event.)

Propagating this source with FUNWAVE-TVD in grid G1a, after 9 h, we find the maximum tsunami surface elevation plotted in Fig. 3c. Maximum tsunami impact is clearly aimed at the general area of the NSOH; results in this coarse grid indicate that maximum elevations would be on the order of 1 m on the Caribbean Islands and the NSOH, which is quite moderate. These values, however, will be refined in the nested-grid, higher-resolution simulations.

3.1.2 Local PRT seismic source

We model a $M_w = 9$ seismic source in the PRT, corresponding to a large earthquake rupturing the 600-km long part of the trench orientated W–E north of Puerto Rico (Figs. 1, 4). As discussed above, this represents a conservative extreme tsunami scenario (PMT) for the PRT, but a similar tsunami could be generated on the western side of the trench by a smaller magnitude event causing the same slip over a smaller section of the PRT. Unlike the initial work of Grilli et al. (2010), where only one fault plane was used (600 by 150 km), to better model the curved geometry of the trench, similar to Grilli and Grilli (2013b) and Grilli et al. (2015b), we use 12 individual sub-fault planes with parameters obtained from the SIFT database ("Short-term Inundation Forecast for Tsunamis"; Gica et al. 2008). Each sub-fault

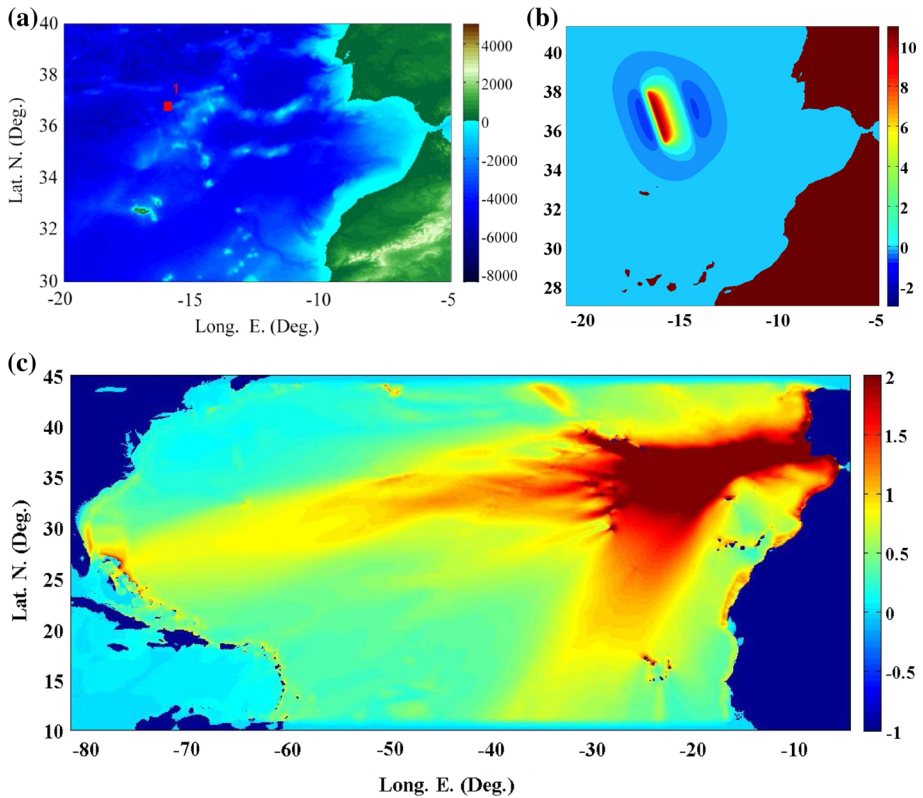


Fig. 3 Far-field tsunami source for a M_w 9.0 earthquake in the Azores convergence zone (Madeira Tore Rise; LSB) : **a** source location and surrounding bathymetry; **b** initial surface elevation computed with Okada’s (1985) method (from Grilli and Grilli 2013a; Grilli et al. 2015b); and **c** envelope of maximum tsunami surface elevation computed with FUNWAVE-TVD in 1 arc-min grid G1a after 9 h of propagation (Fig. 1; Table 1). (All color scales are in meter.)

corresponds to a so-called SIFT unit source of magnitude $M_w = 7.5$, length $L = 100$ km, width $W = 50$ km and a slip of 1 m (with these parameters, we find $\mu = 35.6$ GPa); the location, depth and orientation of each sub-fault plane (strike, dip and rake angles) are based on the local geology (see details in Grilli and Grilli 2013b). The slip of each sub-fault is scaled for the total magnitude of the event to be $M_w = 9$, or $M_o = 3.162 \times 10^{22}$ N m; thus, $S = (M_o/12)/(LW\mu) = 14.8$ m. Parameters for the 12 SIFT sub-fault planes are listed in Table 2. Using these parameters in Okada’s model, we compute the initial surface elevation shown in Fig. 4a, which varies between -4 and $+8$ m. Figure 4b shows the surface elevation simulated in grid G1b, after 30 min of propagation of this source using FUNWAVE-TVD. We see that a fairly narrow and directional train of the largest tsunami waves is aimed almost directly north (toward the upper USEC; see Grilli et al. 2010, 2015b), with some additional westward propagation of waves with an elevation on the order of 1 m that are starting to impact the NSOH and the Caribbean Islands. This directionality supports the above statement regarding a smaller magnitude earthquake in the western side of the PRT causing similar tsunami impact on the NSOH. The envelope of maximum tsunami surface elevation computed after 3 h of propagation is plotted in

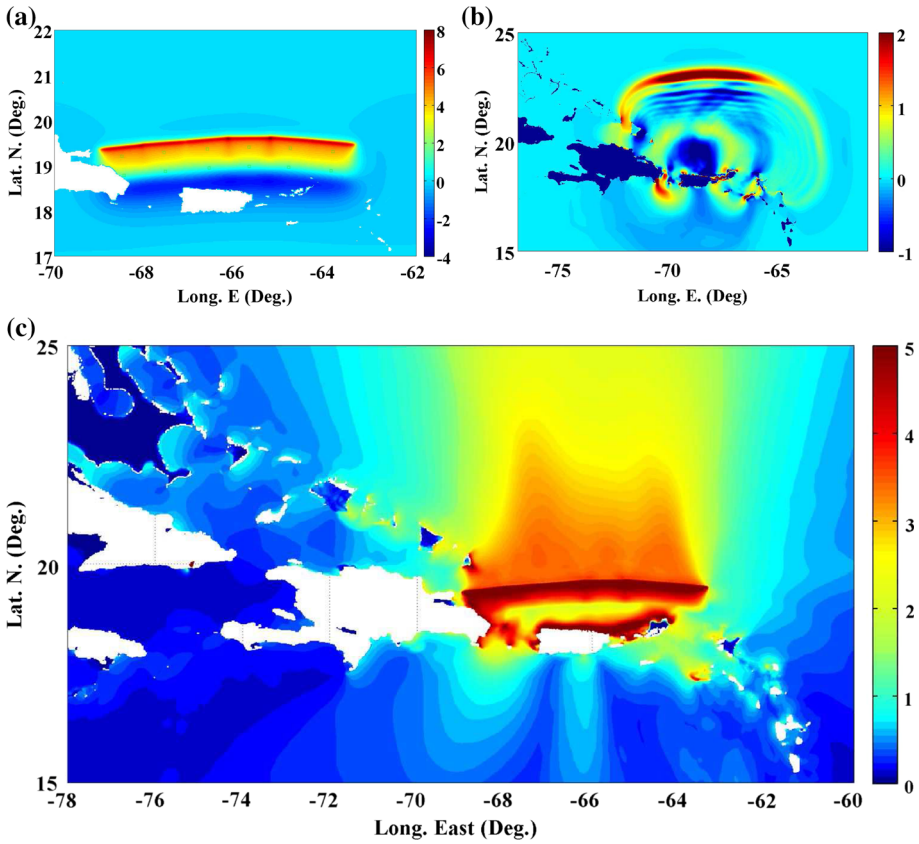


Fig. 4 Local tsunami source for a M_w 9.0 earthquake in the Puerto Rico Trench (PRT; Grilli et al. 2010; Grilli and Grilli 2013b; Grilli et al. 2015b) : **a** initial surface elevation computed with Okada's (1985) method based on parameters listed in Table 2; and simulations with FUNWAVE-TVD in 1 arc-min grid G1b (Table 1) of **b** instantaneous (30 min) and **c** envelope of maximum surface elevations after 3 h of propagation. (All color scales are in meter.)

Table 2 Parameters for a PRT M_w 9 seismic event represented by 12 SIFT fault planes (adapted from Gica et al. 2008), with in addition for each plane: Length $L = 100$ km, Width $W = 50$ km, Dip $\delta = 20^\circ$, Rake $\gamma = 90^\circ$, Slip $S = 14.8$ m, and Coulomb modulus $\mu = 35.6$ GPa

No.	Locator	Lat. (N°)	Lon. (W°)	Depth (km)	Strike (°)
1	atsza48	18.887	63.88	22.1	95.37
2	atszb48	19.3072	63.8382	5	95.37
3	atsza49	18.965	64.8153	22.1	94.34
4.	atszb49	19.3859	64.7814	5	94.34
5	atsza50	18.9848	65.6921	22.1	89.59
6	atszb50	19.4069	65.6953	5	89.59
7	atsza51	18.9484	66.5742	22.1	84.98
8	atszb51	19.3688	66.6133	5	84.98
9	atsza52	18.8738	67.5412	22.1	85.87
10	atszb52	19.2948	67.5734	5	85.87
11	atsza53	18.7853	68.4547	22.1	83.64
12	atszb53	19.2048	68.5042	5	83.64

Fig. 4c; while results in this coarse grid indicate that most of the NSOH would experience up to 1.5 m surface elevation, which is moderate, its eastern end and the Island of Puerto Rico would be impacted by much larger waves, up to 5 m in elevation. These values, however, will be refined in the nested-grid, higher-resolution simulations.

3.1.3 Far-field CVV collapse source

The surface elevation and velocity of the 450 km³ CVV flank collapse source (from Abadie et al. 2012; Tehranirad et al. 2015) are shown 20 min after the event in Fig 5a, b, respectively; at this time, the tsunami source appears as a series of concentric waves, with elevations ranging between -100 and $+100$ m horizontal velocity modules of up to 4 m/s, and a clear directionality in the WSW direction (about 20° south of West). Figure 5c shows the instantaneous surface elevation computed using FUNWAVE-TVD in grid G1a (Fig. 1), around Hispaniola after 7 h 20 min of propagation. Despite the long propagation distance from the source, a train of several large waves, with elevations approximately in the range -6 m to $+8$ m is approaching the NSOH; this is consistent with results reported by Tehranirad et al. (2015) who noted that, for this CVV source, trains of 3–5 large waves of period 9–12 min would be approaching southern Florida after about 8 h of propagation. The envelope of maximum surface elevation computed after 8 h of propagation is plotted in Fig. 5d, e, for the entire northern Atlantic Ocean basin and as a zoom-in onto the area of Hispaniola, respectively; results in this coarse grid indicate that most of the NSOH would experience up to 4–8 m surface elevation. These values, however, will be refined in the nested-grid higher-resolution simulations. (It should be noted that the very large elevations in (d, e) west of Hispaniola are spurious and due to grid coarseness; these disappear in finer nested grids.)

3.1.4 Near-field seismic sources (NHTF, SF)

We simulate two of the near-field seismic sources recommended by the Port-au-Prince workshop of experts (UNESCO 2013):

1. A M_w 8.0 rupture of the SF similar to the 1842 event (referred to as scenario #1 in UNESCO 2013); as discussed before, this could be considered as a 500-year event. The SF is a strike-slip fault, which has a total length of about 300 km and is orientated nearly west–east (Fig. 1b), from the western extremity of Cuba to Turtle Island, north of the NSOH (strike $\simeq 90^\circ$); eastward of Turtle Island, the fault is orientated parallel to the western part of the NSOH (strike $\simeq 100^\circ$) and then crosses the land itself. For this “strike-slip” fault, UNESCO (2013) recommended the parameters listed in Table 3, where the fault is divided into two segments, with approximately the strike angles mentioned above and a total length of 328 km; the dip angle is 90° and rake angle 0° for each segment. Using the standard value $\mu = 33$ GPa for the Coulomb modulus, the moment magnitude is: $M_o = 1 \times 10^{21}$ N m, yielding a slip: $S = M_o / ((L_1 + L_2)W\mu) = 4.6$ m, which is slightly less than the 5-m slip recommended in the UNESCO (2013) report; hence, using this value of slip instead, we find a magnitude M_w 8.02, which we use here. Given these parameters, the part of the SF that is inland would not generate a significant tsunami for our geographic area of interest and, hence, one could have limited the fault here to the part located in the ocean, off of

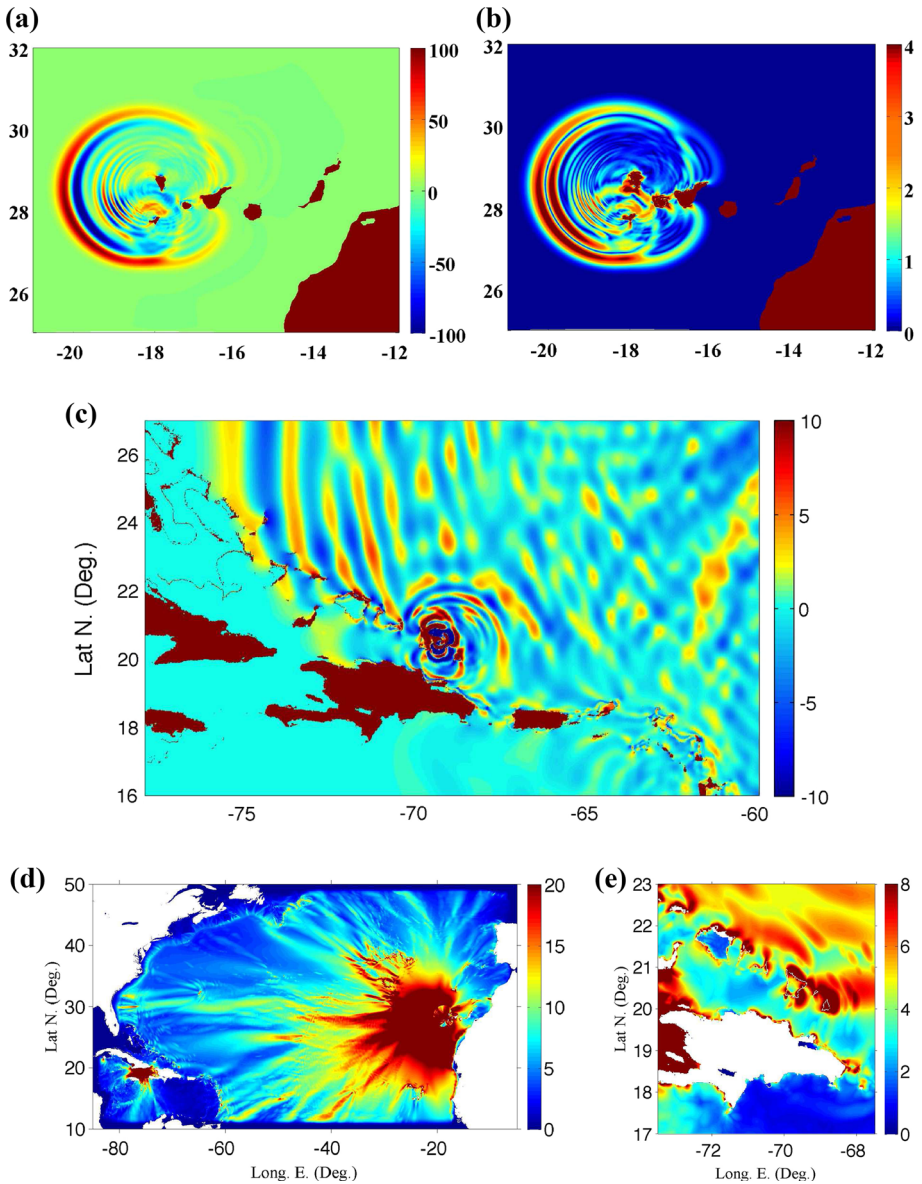


Fig. 5 Far-field tsunami source for a 450 km^3 Cumbre Vieja Volcano flank collapse (CVV): **a, b** tsunami source elevation (meter) and horizontal velocity module (m/s) after 20 min of simulations since the event (Abadie et al. 2012; Tehranirad et al. 2015); surface elevation (meter) computed with FUNWAVE-TVD in 1 arc-min grid G1a (Fig. 1; Table 1), **c** instantaneous after 7 h 20' of propagation, **d, e** envelope of maximum surface elevation after 8 h of simulations. (Note that the very large elevations that appear in subplots **d, e**, west of Hispaniola, are spurious and due to grid coarseness; these disappear in simulations with finer nested grids and do not affect the one-way coupling method.)

the NSOH, which is only about 100 km long. Nevertheless, following the recommendations of UNESCO (2013), we first considered the entire fault length with the recommended vertical dip and zero rake and computed the initial surface

elevation with Okada’s (1985) method; as could be expected for a strike-slip fault, with these parameters, we only found a very small initial tsunami of less than ± 0.2 m elevation (not shown here).

To be conservative and increase tsunami generation on the NSOH, considering geological uncertainties, we then varied the dip and rake angles by $\pm 20^\circ$, with respect to the recommended values of Table 3. Figure 6 thus shows the initial surface elevation (i.e., tsunami source) computed using the Okada (1985) method based on parameters in Table 3, but for 5 (rake, dip) combinations with : (a) $0^\circ, 70^\circ$; (b) $20^\circ, 70^\circ$; (c) $-20^\circ, 70^\circ$; (d) $20^\circ, -70^\circ$; and (e) $-20^\circ, -70^\circ$. These were the parameter combinations that we found generated the largest initial surface elevations. Nevertheless, the figures show that these are negligible on the eastern part of the NSOH (including the Puerto Plata area) and small or moderate along and off of the western part of the NSOH (including the Cape Haitien area), except in between the NSOH and Turtle Island, due to an artifact of the Okada method where the two specified fault segments superimpose; hence, this local increase in seafloor deformation can be ignored. As could be expected, initial tsunami elevations are the smallest for the strike-slip case of Fig. 6a, in between $+0.2$ and -0.2 m near the NSOH, similar to values found for the original scenario #1. For the positive rake cases of Fig. 6b, d, ignoring the artifact south of Turtle Island, we find a maximum elevation of less than $+0.8$ m along the NSOH, with a similar maximum depression slightly offshore. This should generate waves essentially moving away from the NSOH, for which the impact onshore would be less than the initial value. Finally, for the negative rake cases of Fig. 6c, e, and again ignoring the artifact south of Turtle Island, the initial wave

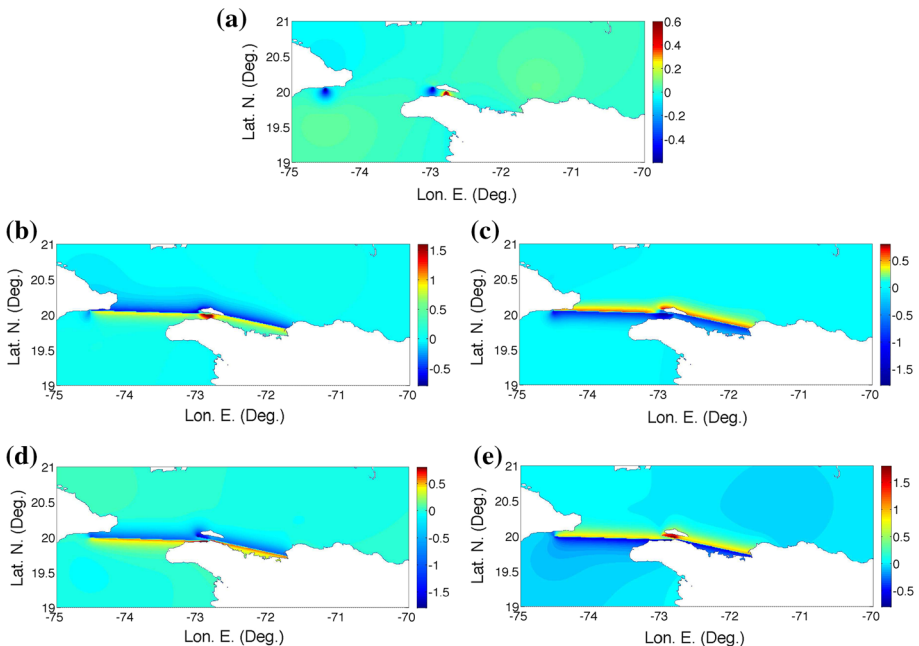


Fig. 6 Near-field seismic tsunami sources: initial surface elevation (color scale in meter) computed with Okada’s (1985) method, for M_w 8.0 seismic events in the SF, based on UNESCO (2013) scenario #1, with parameters listed in Table 3, but using 5 modified (rake, dip) combinations: **a** $0^\circ, 70^\circ$; **b** $20^\circ, 70^\circ$; **c** $-20^\circ, 70^\circ$; **d** $20^\circ, -70^\circ$; and **e** $-20^\circ, -70^\circ$

Table 3 Parameters for a M_w 8.0 seismic event in the SF (scenario # 1 from UNESCO 2013), represented by 2 sub-fault planes, with in addition for each plane: Width $W = 20$ km, Dip $\delta = 90^\circ$, Rake $\gamma = 0^\circ$, Slip $S = 5$ m, and Coulomb modulus $\mu = 33$ GPa

No.	Lat. (N°)	Lon. (W°)	Depth (km)	Strike (°)	Length (km)
1	20.000	73.639	5	91.7	179
2	19.812	72.088	5	102.9	149

elevations are roughly inverted, with a maximum elevation of less than +0.8 m offshore along the NSOH and a similar maximum depression onshore. Here, one would expect a short-wave propagation and shoaling onshore, but considering the modest initial wave amplitudes and small wavelength, this should only cause a small impact on the NSOH, negligible as we shall see in view of that of the PRT, CVV and NHTF sources. Based on this, we elected not to further model this source, since its impact would evidently be small on the NSOH, in the context of a comprehensive tsunami hazard assessment from all possible sources and corresponding PMTs.

2. An extreme M_w 8.7 rupture of the NHTF (referred to as scenario #3 in UNESCO 2013), which outlines the subduction zone of the North American plate under the Gonave micro-plate (Fig. 1b), representing a much larger seismic event than the 1946 earthquake that struck eastern Hispaniola (Dolan and Wald 1998; Benford et al. 2012) (i.e., one that would cause a much longer rupture of the NHTF); as discussed before, this could be considered as a 2500-year event.

For this event, based on the study of the focal mechanism for the 1946 earthquake by Dolan and Wald (1998) and GPS results by Calais et al. (2010), UNESCO (2013) recommends the fault plane parameters listed in Table 4, where the fault is divided into three segments that match the geometry of the fault trace on the seafloor, approximately marked in Fig. 1b, with a total length of 623 km; the dip angle is 21° and rake angle 90° for each segment. Note that the definition of the sub-faults' geometry was not standard in UNESCO's (2013) report, and it was assumed that the values listed were those of the trace of the northern part of each sub-fault on the seafloor, from which the coordinates of the center and dimensions and depth at the center of each sub-fault plane listed in the table were calculated; otherwise, the seafloor deformation for this event would have been moved too far north onto the non-subducting part of the seafloor; not proceeding this way would also have been inconsistent with the specified depth for the event. UNESCO (2013) further indicates that the rake angle of the NHTF segments may vary in the range 70° – 90° . However, following Gica et al. (2008) who note that tsunami generation is larger for a 90° rake, we only used (and listed) this value in Table 4.

Using the standard value $\mu = 33$ GPa for the Coulomb modulus and assuming a M_w 8.7 magnitude, i.e., a moment $M_o = 1.122 \times 10^{22}$ N m, based on the values listed in Table 4, we find a slip: $S = M_o / ((L_1 + L_2 + L_3)W\mu) = 9.2$ m, which is slightly less than the 10-m slip recommended in the UNESCO (2013) report; hence, using this value of slip instead, we find a magnitude M_w 8.72, which we use here. Figure 14a shows the initial surface elevation (i.e., tsunami source) computed using the Okada (1985) method based on parameters in Table 4. Elevations vary in the range -1.5 to 5.0 m, which in view of the proximity of the NSOH should lead to a significant coastal impact.

Now, considering the possibility that, for such a large seismic event, either the entire length of the fault (which is considerable here) would not rupture at once and/or slip would

be larger in some parts of the ruptured areas than others (a much likelier possibility than assuming a uniform slip over such a large surface area), we designed an alternate scenario, in which a larger slip occurs over a shorter fault length. Our approach to do so was based on two considerations. First, we noted that the locations given in UNESCO (2013) for the three sub-fault planes led to a seafloor deformation (in Fig. 14a) that has a large uplift north of the assumed trace of the NHTF on the seafloor and a subsidence south of it. However, for the two large earthquakes and tsunami events that occurred in the last decade, in the Indian ocean in 2004 (M_w 9.2) and in Japan in 2011 (M_w 9.0), in subduction zones whose fault planes had similar rake and dip angles as in the present case (see, e.g., Grilli et al. 2007; Ioualalen et al. 2007; Grilli et al. 2013c), it was observed that the majority of seafloor deformation (and corresponding slip) was located within the subduction zone and thus in between the fault trace on the seafloor (e.g., the “Japan Trench”) and the considered island/overlying plate (i.e., Indonesia or Honshu). Second, we observed that in important historical seismic events (such as the two earthquakes discussed above) that occurred over large fault areas (similar to the 693 by 59 km rupture area considered here), both the ultimate slip and resulting seafloor deformation were very inhomogeneous in space. For instance, there was an asperity (where very large slip occurred) in the rupture area of the 2004 Indian Ocean event, leading to a much larger impact in the nearest region of Banda Aceh (over 40-m runup), and for the 2011 Japan event a seafloor area with very large deformation off of Sanriku also led to the largest observed runups in Honshu (up to 40 m; Shimozono et al. 2014).

Hence, to account for these historical observations in the present case while designing the most conservative (and hence likeliest most severe) tsunami for the NSOH resulting from scenario #3, without performing many different simulations (e.g., with different slip distributions), and considering the orientation almost parallel to shore of the NHTF, which leads to the generation of tsunami waves that are essentially propagating in a north to south direction, we developed the following alternate scenario:

- To slightly move southward the area of seafloor deformation for this event, and have a nearly zero deformation in the area of the trace of the NHTF on the seafloor (as, e.g., seen for the Indian Ocean 2004 and Japan 2011 events), we based this scenario on four local SIFT sub-fault planes (Gica et al. 2008), which are located further south than the three segments of scenario #3. These SIFT sub-fault planes are used by NOAA for tsunami forecasting in the region and are referred to as “Atlantic Subduction Zone” (atsz) segments b55–b58 and have parameters listed in Table 5; they all have a length $L = 100$ km, width $W = 50$ km and as indicated before represent each a M_w 7.5 event given a 1-m slip.
- To account for the possibility of larger slip occurring in some areas of the NHTF off of the NSOH, we considered a shorter 400 km length of the rupture area and increased slip to keep the same M_w 8.7 magnitude; the rupture area thus spans the length of the 4 selected SIFT sub-fault planes, which overlap the entire NSOH. Despite the fairly shallow depth (5 km) recommended for the rupture of these SIFT sub-faults, we use the standard value of the Coulomb modulus, $\mu = 35.6$ GPa, recommended by NOAA in subduction zones, which leads to a scaled up slip value for the 400 by 50 km rupture area and a M_w 8.7 event, or $M_o = 1.122 \times 10^{22}$ N m: $S = (M_o/4)/(4LW\mu) = 15.76$ m. This slip value is about 50 % larger than that of scenario #3.

It should be pointed out that, in developing this alternate scenario for the purpose of tsunami hazard assessment, we do not aim at defining a more realistic seismic source, but instead we are

building an event that would be a composite of many failures, in which a larger slip (by up to 50 %) would occur in some unknown parts of the ruptured area and not others, in the original, longer (693 km), fault parameterized in UNESCO's (2013) scenario #3. The tsunami resulting from this alternate scenario should thus be the worst-case scenario for all the areas of the NSOH, with respect to the extreme NHTF event. This single scenario approach, rather than simulating many different cases with non-uniform slip over a longer fault, is possible here because, in all cases, the incident waves are propagating more or less in the same north to south direction. Thus, we can build a worst-case scenario for a 50 % non-uniform slip as a single scenario, in which the fault is reduced in length and the slip is increased everywhere.

Figure 14b shows the initial surface elevation (i.e., tsunami source) for the alternate NHTF scenario, computed using Okada's (1985) method based on parameters in Table 5. Elevations vary in the range -2.5 to 9.0 m, which as could be expected is larger than for scenario #3 by about 50 % and, in view of the even closer proximity of the NSOH, should lead to a coastal impact also more severe than for scenario #3. This will be verified in simulations with FUNWAVE-TVD in the G22b,c grids.

3.2 Regional and nearshore Tsunami propagation

For each selected tsunami source, we present results of tsunami simulations with FUNWAVE-TVD in the regional Cartesian grids G22a, b, c (205-m resolution; Table 1), in the

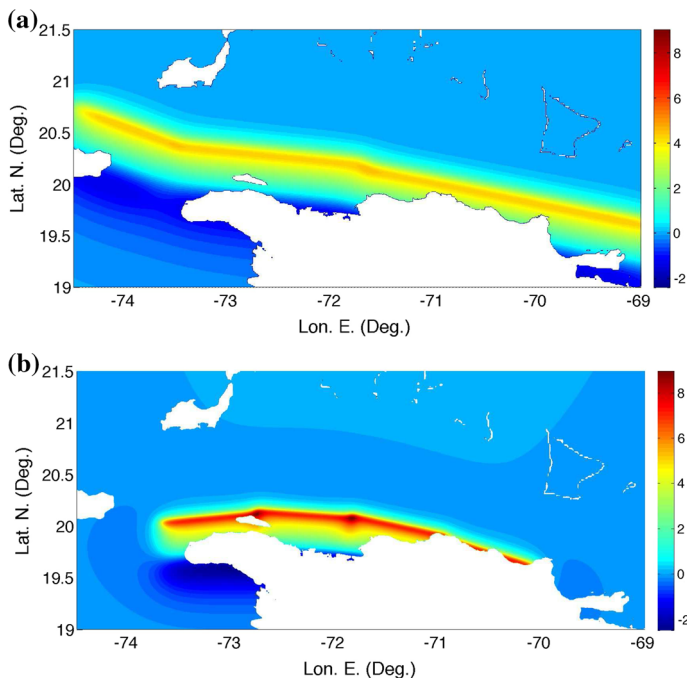


Fig. 7 Near-field seismic tsunami sources. Initial surface elevation (*color scale in meter*) computed with Okada's (1985) method for a M_w 8.7 seismic event in the NHTF based on : **a** the three-segment source from UNESCO's (2013) scenario #3 (Table 4); and **b** an alternate scenario with a four-segment source based on SIFT sub-faults (Table 5). (Note, for comparison, the same surface area and color scale are used in each subplot.)

Table 4 Parameters for a M_w 8.7 seismic event in the NHTF (scenario # 3 from UNESCO 2013; based in part on Dolan and Wald 1998 and Calais et al. 2010), represented by 3 sub-fault planes, with in addition for each plane: Width $W = 59$ km, Dip $\delta = 21^\circ$, Rake $\gamma = 90^\circ$, Slip $S = 10$ m, and Coulomb modulus $\mu = 33$ GPa

No.	Lat. (N°)	Lon. (W°)	Depth (km)	Strike (°)	Length (km)
1	20.3554	74.1050	10.6	111.3	111
2	20.0557	72.6331	10.6	96.6	195
3	19.6351	70.2698	10.6	102.6	317

Table 5 Parameters for a M_w 8.7 seismic event in the NHTF represented by 4 SIFT sub-fault planes (Gica et al. 2008), with in addition for each plane: Length $L = 100$ km, Width $W = 50$ km, Dip $\delta = 20^\circ$, Rake $\gamma = 90^\circ$, Slip $S = 15.76$ m, and Coulomb modulus $\mu = 35.6$ GPa

No.	Locator	Lat. (N°)	Lon. (W°)	Depth (km)	Strike (°)
1	atszb55	19.5386	70.5647	5	108.19
2	atszb56	19.7971	71.4386	5	102.64
3	atszb57	19.9047	72.3206	5	94.2
4	atszb58	19.8698	73.2022	5	84.34

form of envelopes of maximum surface elevation and time series of surface elevation at many stations along the boundary of the two finer TELEMAC grids centered around Cap Haitien and Puerto Plata (Fig. 2b). Based on these time series and similar time series of horizontal currents, detailed computations of tsunami coastal impact will be performed in TELEMAC (presented in the next section). (Note that at both Cap Haitien and Puerto Plata, the offshore boundary of the TELEMAC grid is located in deep enough water for the high-resolution model grid to cover any shallow shoals or fringing reefs that could be located further onshore.) For the LSB, CVV and PRT sources, simulations are performed in three levels of nested grid by one-way coupling, based on results in the G1a,b and G2 grids (results of the latter grid are not detailed here). For the near-field sources, simulations are directly performed in the G22b,c grids.

3.2.1 Far-field (LSB, CVV) and local (PRT) sources

Figures 8, 9, and 10 show the envelopes of maximum surface elevations computed in the 205-m resolution grid G22a for the LSB, PRT and CVV sources. In each case, results are shown in panel (a) for the entire grid and in panels (b) and (c) for zoom-ins around the two critical areas of Cap Haitien and Puerto Plata. As expected from earlier simulations, the maximum coastal impact occurs for the CVV source, with 9- and 20-m maximum runup at each of the sites, respectively. The next largest impact is caused by the PRT source, with 3 and 4 m maximum runup at each site, and finally LSB, with only 1 and 0.7 m maximum runup at each site.

These runup values are confirmed in the time series of Fig. 11 which, for each of the 3 sources, shows surface elevations computed in Grid22a at all the points (stations) located along the boundary of the two finer TELEMAC grids centered around Cap Haitien and Puerto Plata (Fig. 2b). Note that while arrival times for the LSB and CVV far-field sources are over 6–7 h at both sites, those of the PRT source are within 1 h at both sites, confirming its earlier characterization as a “local” source. These time series, together with those for



Fig. 8 Far-field LSB M_w 9.0 seismic tsunami source: **a** envelope of maximum surface elevation computed in grid G22a after 9 h of propagation; zoom around **b** Cap Haitien, and **c** Puerto Plata (both marked by a black square). (All color scales are in meter.)

the corresponding horizontal velocity components (not shown here), are used to force the TELEMAC simulations.

3.2.2 Near-field (NHTF) sources

Figures 12 and 13 show envelopes of maximum surface elevations computed with FUN-WAVE-TVD in the 205-m resolution grids G22c and G22b, for the NHTF M_w 8.7 near-field tsunami sources from: (a) scenario #3 (UNESCO 2013), and (b) the alternate SIFT-based scenario, respectively. In each case, results are shown in panel (a) for nearly the entire grid and in panels (b) and (c) as zoom-ins around the two critical areas of Cap Haitien and Puerto Plata (note that for comparison, these are plotted with the same color scale in both Figs. 12 and 13). These simulations are initialized with the surface elevations shown in Fig. 7a, b, respectively.

As could be expected from their initial source, the maximum coastal impact occurs for the most intense NHTF source corresponding to the alternate SIFT-based scenario (Fig. 13), which is more compact and closer to the NSOH, with 12- and 8-m maximum runup in the areas of each critical site, respectively. For the source based on scenario #3, the impact is in general reduced to 70–80 % of these values. In particular, in the zoom-ins around the two critical sites, we see that maximum runups are 6 and 8 m at Cap Haitien, and 6.5 and 7 m at Puerto Plata, for each source, respectively.

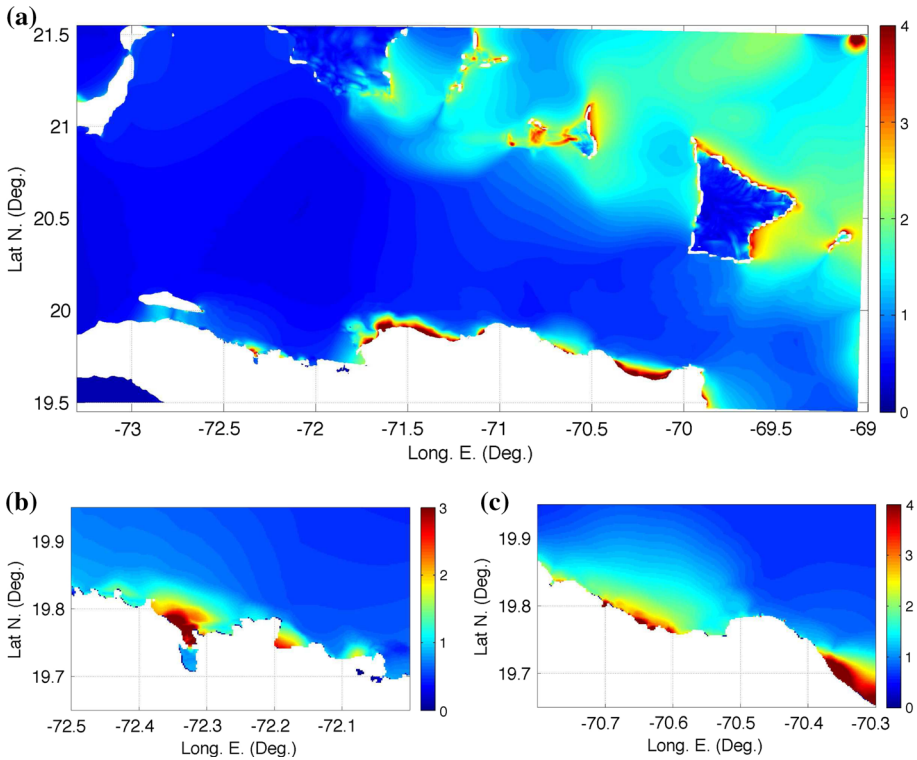


Fig. 9 Local PRT M_w 9.0 seismic tsunami source: **a** envelope of maximum surface elevation computed in grid G22a after 3 h of propagation; zoom around **b** Cap Haitien, and **c** Puerto Plata (see locations in Fig. 8). (All color scales are in meter.)

As for the far-field/local sources, these coastal runup values from the two NHTF near-field source scenarios are confirmed in the time series of Fig. 14 which, for each source, show surface elevations computed in Grid22c,b at all the points (stations) located along the boundary of the two finer TELEMAC grids centered around Cap Haitien and Puerto Plata (Fig. 2b). Off of Cap Haitien, maximum elevations of 5.8 and 7.8 m occur after 8.8 and 6.9 min, and off of Puerto Plata, 5 (5.5)- and 6.8-m elevations occur after 4.5 (17.1) and 1 min, for each source, respectively (numbers in parentheses correspond to characteristics of a second slightly larger wave that occurs in Puerto Plata for scenario #3, 12.5 min after the first wave).

Overall, the time series in Fig. 14 indicate that, for the NHTF sources:

- Waves in the incident tsunami off of Cap Haitien are 34 % higher with the alternate SIFT-based scenario than for scenario #3 and arrive 2 min earlier, due to the greater proximity of the source to shore.
- Waves in the incident tsunami off of Puerto Plata are 36 (24) % higher with the alternate SIFT-based scenario than for scenario #3 and arrive 3.5 (16) min earlier, due to the greater proximity of the source to shore (results in parentheses correspond to the second slightly larger wave in the wave train).

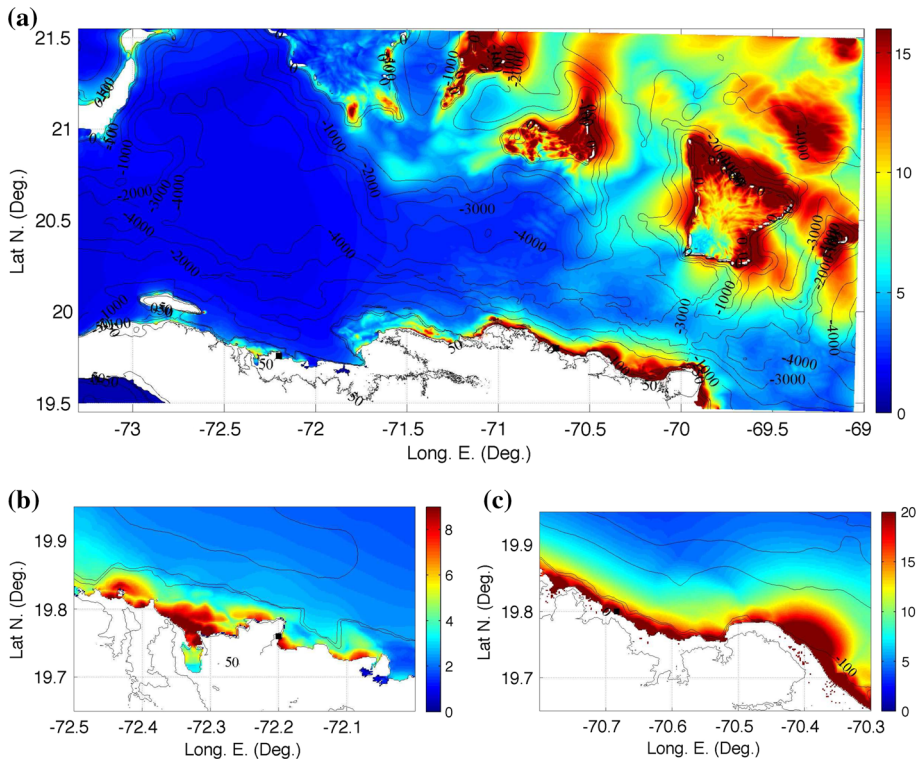


Fig. 10 Far-field CVV 450 km^3 flank collapse tsunami source: **a** envelope of maximum surface elevation computed in grid G22a after 8 h of propagation; zoom around **b** Cap Haitien, and **c** Puerto Plata (locations marked by black squares). (All color scales are in meter.)

Note that these conclusions of a larger coastal impact for the tsunami resulting from the alternate SIFT-based NHTF scenario only apply to the shoreline sections close to each of the two critical sites. In Fig. 12a, we see that, likely due to bathymetric focusing of waves from the scenario #3 source, due to its greater distance from shore, there are some other sections of the coast close to Puerto Plata that show slight increases in runup as compared to the SIFT-based scenario. Hence future assessments of tsunami hazard along the entire NSOH would require selecting which of these two sources causes the largest impact and where.

Based on these results, to perform simulations with TELEMAC of detailed coastal tsunami impact from near-field sources at the two selected sites, we will use the worst-case scenario, which here is the alternate SIFT-based NHTF source. Surface elevation time series of Fig. 14b, together with the corresponding horizontal velocity components (not shown here), will be used to force these TELEMAC simulations.

3.3 Tsunami coastal impact at the two critical sites

The above simulations of near- and far-field sources down to a moderately fine 205-m resolution grid give us a synoptic view of tsunami hazard along the entire NSOH. Thus we see that among the far-field/local sources, CVV causes the largest impact at the two

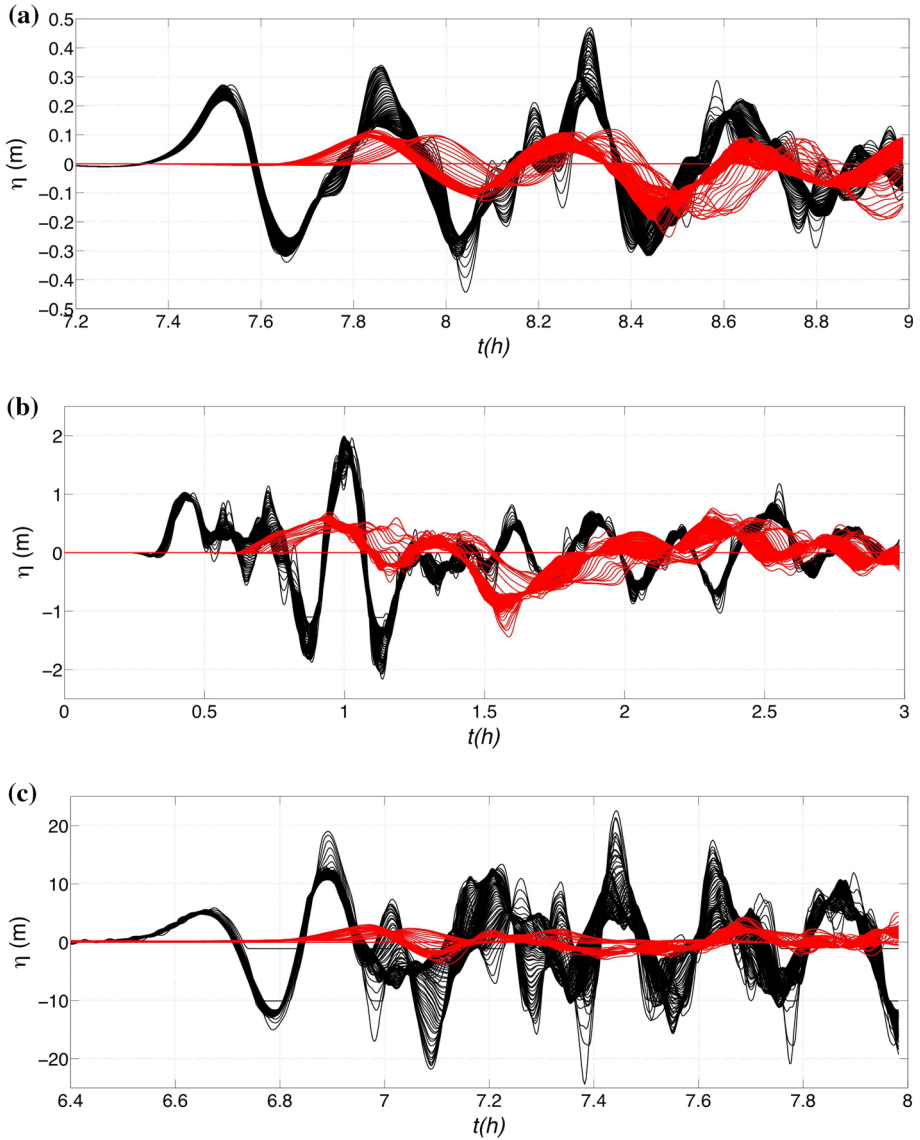


Fig. 11 Time series of surface elevation computed in grid G22a at points along the boundary of the finer TELEMAC grid (Fig. 2b), for the: **a** LSB source; **b** PRT source; and **c** CVV source. *Red curves*: Cap Haïtien; *Black curves*: Puerto Plata. (Note that tsunami arrival times for the PRT source are within 1 h at both site, confirming its characterization as a “local” source.)

selected critical sites, with up to 20-m runup; next, PRT causes up to 4-m runup, and finally, LSB, less than 1 m, which is negligible in view of the other sources. Results also show that a CVV tsunami would reach the NSOH 6.5 h after the event while a PRT tsunami would reach it much quicker, less than 30 min after the earthquake at some locations. This short propagation time, combined with a much lower return period, on the

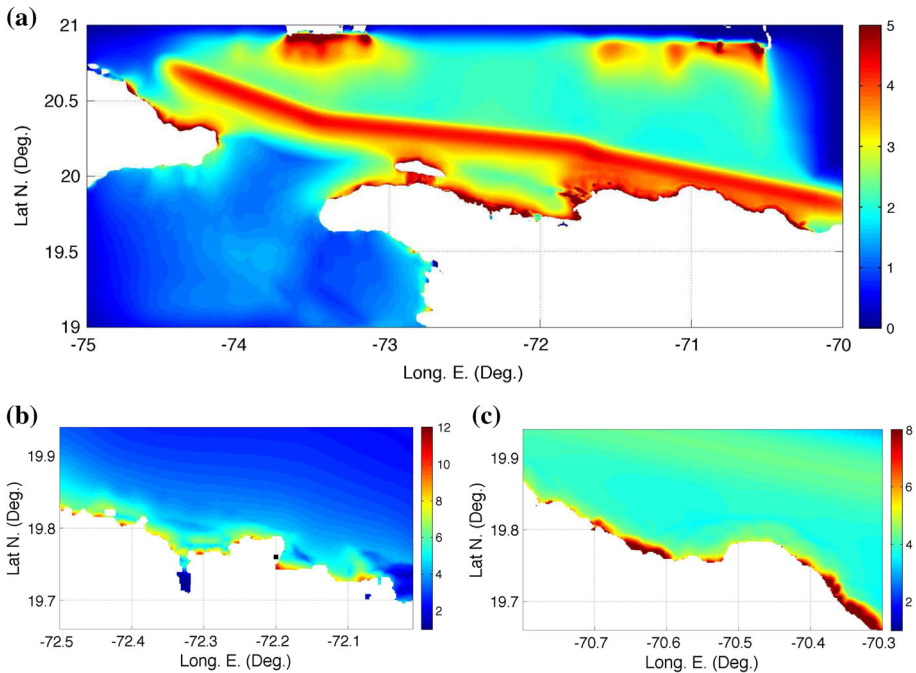


Fig. 12 Near-field NHTF M_w 8.7 seismic tsunami source (scenario #3): **a** envelope of maximum surface elevation computed in grid G22c after 1 h of propagation (note the damping effect of sponge layers around the grid boundary); zoom-in around **b** Cap Haitien, and **c** Puerto Plata (locations marked by *black squares*). (All color scales are in meter.)

order of 600 years (Grilli et al. 2010), as compared to 100,000 years or more for the extreme CVV event (Abadie et al. 2012), makes PRT the most hazardous among the far-field/local tsunami sources for the NSOH (when impact and probability of occurrence are considered).

For the near-field sources, as already indicated, although widespread damage to buildings and infrastructures should be expected from a SF M_w 8 earthquake, a tsunami from this event would be negligible along the NSOH (perhaps 0.5–1-m runup), unless SMFs are triggered as it is suspected may have happened in 1842 (however, SMFs have not been considered in this initial tsunami hazard assessment work). Among the two considered NHTF M_w 8.7 events, the scenario based on the SIFT sub-faults appears to cause the largest impact and to arrive the soonest (a few minutes) at the two selected sites, with 8- and 7-m maximum runup, respectively, and up to 12-m runup elsewhere along the NSOH; a tsunami from scenario #3, however, may cause a slightly larger impact at other sites and hence this case should not be discarded in future detailed studies along the NSOH. Thus, among near-field sources, the NHTF event based on the SIFT sub-faults, whose return period might be on the order of 2500 years, causes the largest tsunami hazard at the two selected sites.

Finally, regarding the so-called Probable Maximum Tsunami (PMT) for the NSOH, considering return period, maximum coastal runup, and arrival time, it appears that the selected NHTF scenario should be considered as the most severe.

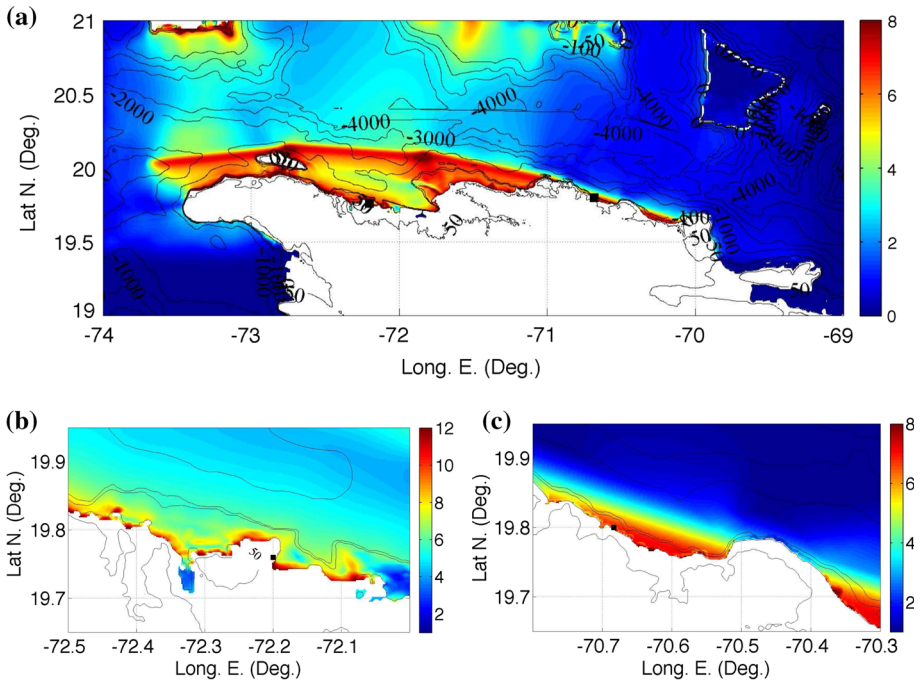


Fig. 13 Near-field NHTF M_w 8.7 seismic tsunami source (alternate SIFT-based scenario): **a** envelope of maximum surface elevation computed in grid G22b after 1 h of propagation (note the damping effect of sponge layers around the grid boundary); zoom around **b** Cap Haitien, and **c** Puerto Plata (locations marked by black squares). (All color scales are in meter.)

Based on the above discussion, the detailed simulations of tsunami coastal impact at the two selected critical sites of Cap Haitien and Puerto Plata were performed in finer-resolution TELEMAC grids for the PRT, CVV, and NHTF (alternate scenario) sources, using the incident tsunamis computed in the G22,a,c grids as offshore boundary conditions (time series in Figs. 11b, c and 14c, and corresponding horizontal velocity). In this paper, however, we only present selected results of these simulations, while more detailed results of coastal impact and vulnerability will be reported on in a future paper. The footprints of the grids used in TELEMAC are shown in Fig. 2b; these are irregular triangular meshes (with 12 to 30 m nearshore resolution) nested in FUNWAVE-TVD’s grids G22a,b,c.

The TELEMAC modeling system was developed by a European consortium of partners led by EDF-R&D (Hervouet 2007) and is dedicated to solving environmental problems in fluid mechanics. The model was specifically designed for performing flood risk assessments, including coastal inundation from storms and in the present context tsunamis. TELEMAC-2D solves the two-dimensional St Venant equations (a.k.a., NSWEs), which describe the nonlinear temporal and spatial evolution of flow depth and depth-averaged current, including effects of bottom friction; the solution is computed with a finite element method (FEM). To more easily refine the grid’s nearshore resolution in very shallow water and follow the terrain features (bathymetry, coastline, port infrastructure, cities and buildings...), TELEMAC uses unstructured triangular meshes; Fig. 15, for instance, shows the grid bathymetry/topography and mesh used around Puerto Plata. Note that topographic

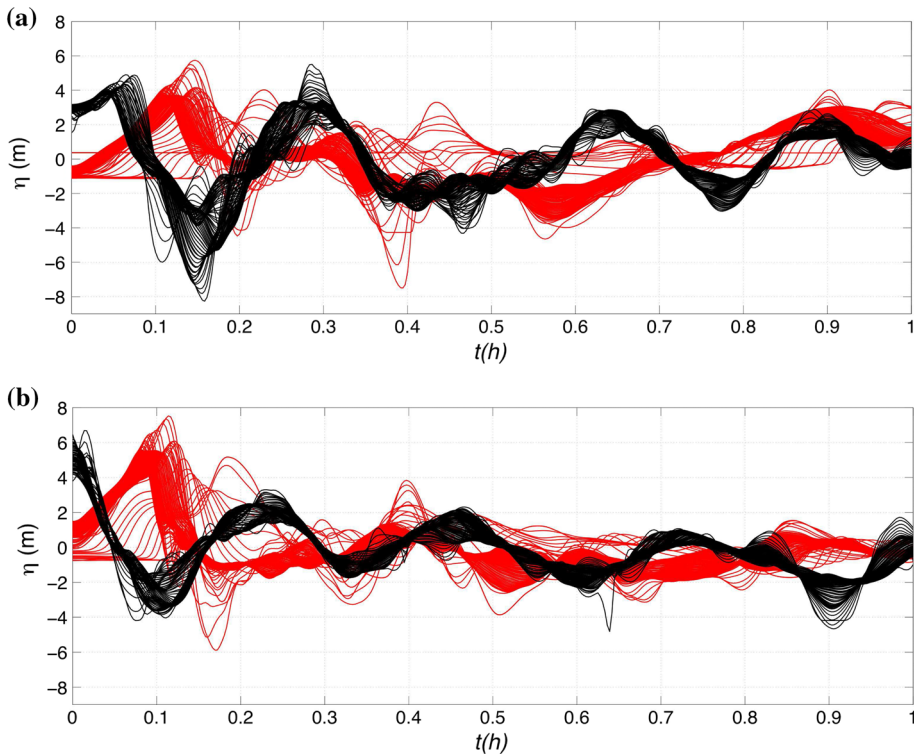


Fig. 14 Time series of surface elevation computed in grids G22c,b at points along the boundary of the finer TELEMAC grid (Fig. 2b), for the NHTF: **a** scenario #3 source; **b** alternate SIFT-based scenario. *Red curves*: Cap Haitien; *Black curves*: Puerto Plata. (Note the two subplots have the same *horizontal and vertical scales*.)

data at the two critical sites include man-made buildings and infrastructures that were added above the standard bare earth topography. Elsewhere on the NSOH, bare earth topography was used, in particular in all of FUNWAVE-TVD's grids. Also note that fringing reefs were present at both critical sites. These were included in TELEMAC's bathymetric model based on the following method: (1) the general bottom bathymetry up to shore was developed based on the best bathymetric data set available without reefs; then (2) reefs were identified using the most recent satellite imagery available. Their location and shape were then added onto the bathymetry and a new digital terrain map was created, which included the reefs themselves as well as free zones, in particular, the deeper channels in between reefs where waves will propagate faster. The offshore boundary of the model grid was placed far enough away from shore to not intersect any reef.

As indicated, TELEMAC is forced at its offshore boundary with results from FUNWAVE-TVD's highest resolution 205-m Cartesian grids. The model then computes tsunami propagation in shallow water, over land, and within the cities at the two critical sites. Such detailed, site specific, results of tsunami flow depth and velocity can be used to support decisions with regard to mitigation and future crisis management. Figure 16 shows an example of computed maps of maximum inundation depth and velocity module, for the M_w 8.7 NHTF source around Cap Haitien (alternate SIFT-based scenario; case of

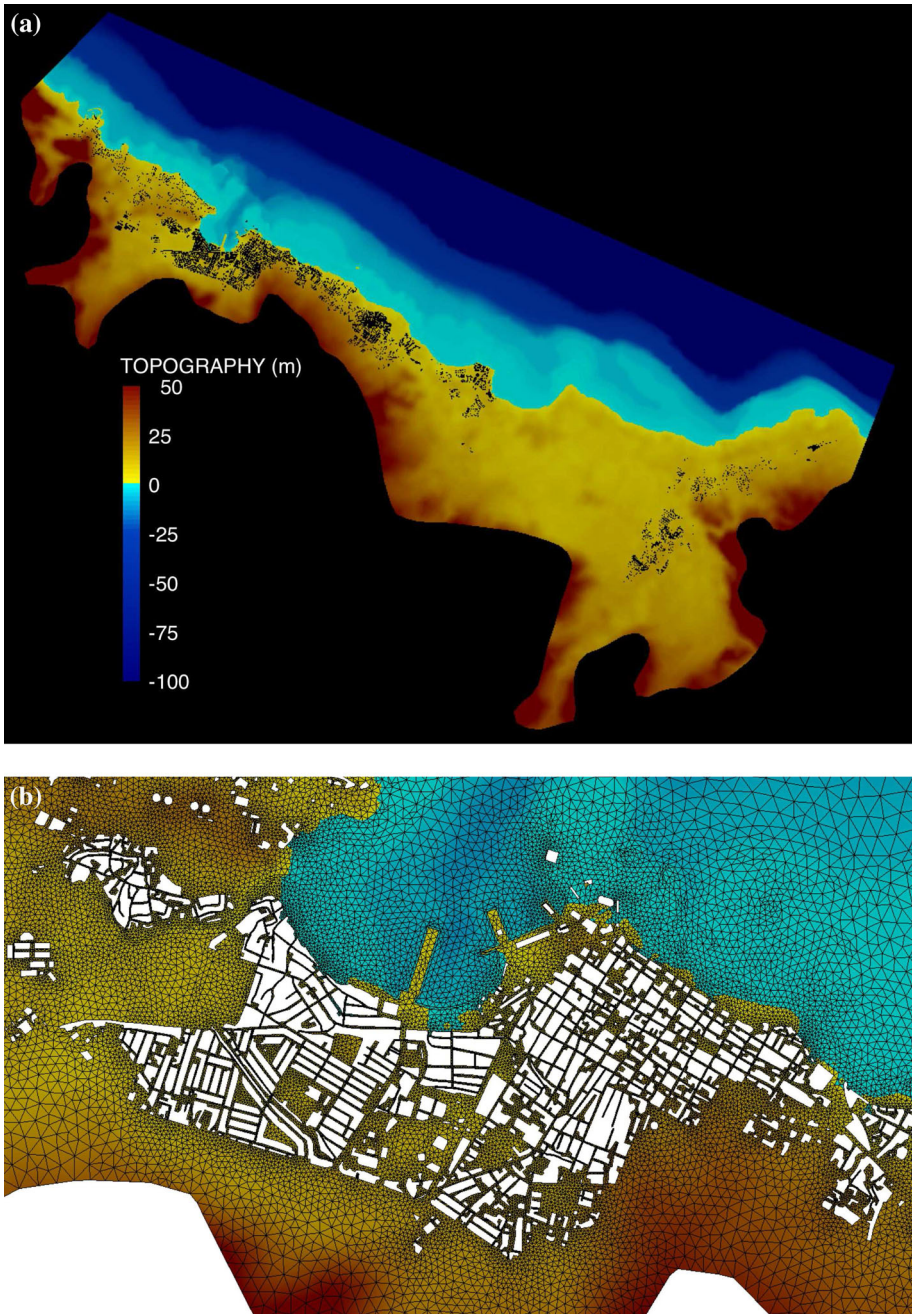


Fig. 15 Grid used by TELEMAC around Puerto Plata (footprint of the grid is also shown in Fig. 2b; *color scale* indicates bathymetry and topography): **a** entire grid bathymetry/topography; **b** zoom-in on the center of the city with superimposed irregular FEM grid (12–30-m-size triangular elements). Note that the mesh includes and is defined around buildings and infrastructures (marked in *white*), i.e., it is not based on a bare land DEM

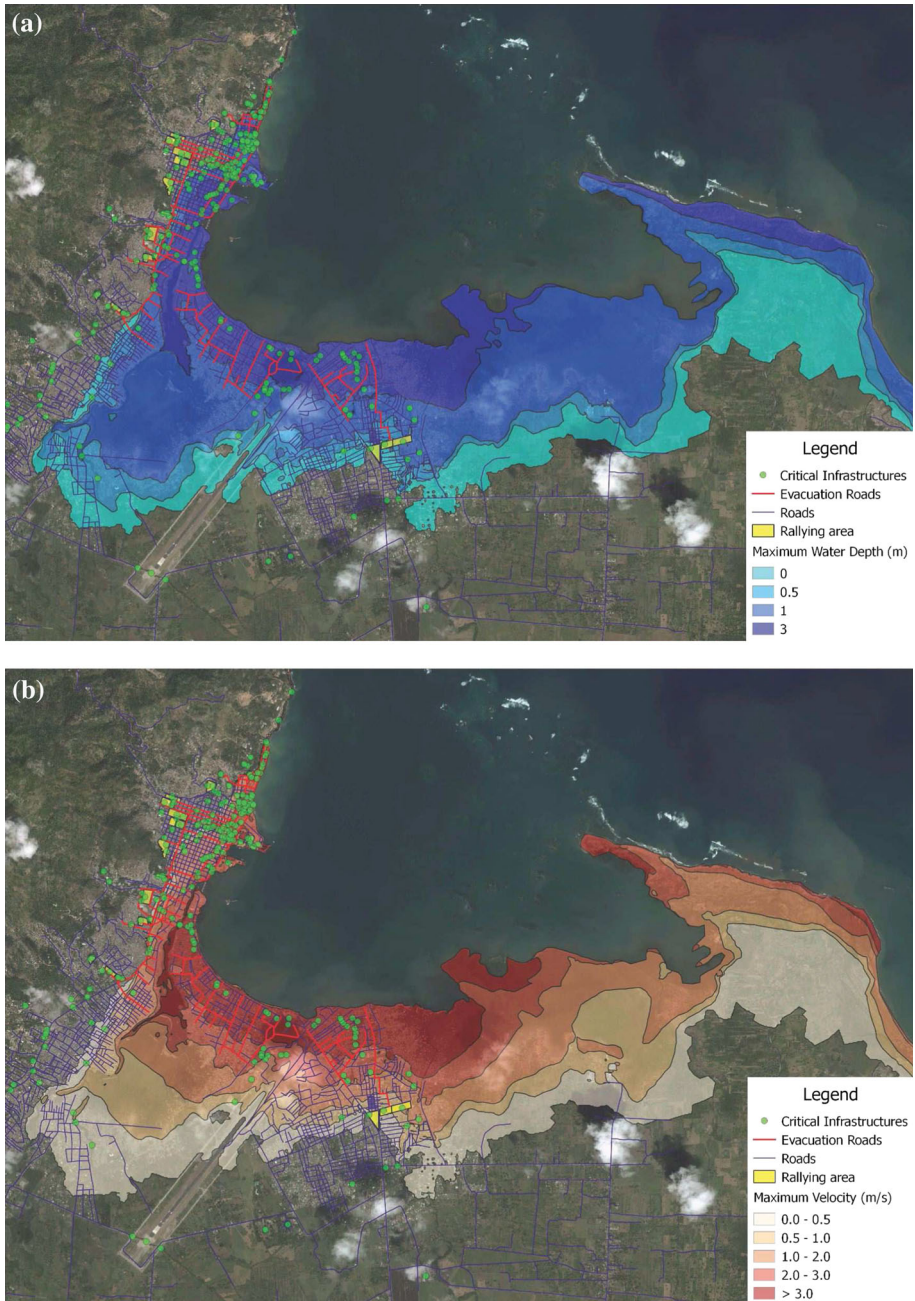


Fig. 16 Maximum inundation **a** and velocity module **b** computed with TELEMAC-2D around Cap-Haïtien, in a 12–30-m resolution irregular FEM grid (the footprint of the grid is shown in Fig. 2b), for the M_w 8.7 near-field seismic NHTF source (alternate SIFT-based scenario; case of Fig. 13b), which is the PMT for the site. Various critical infrastructures are marked on the map in order to estimate their vulnerability to tsunami impact

Fig. 13b), which also identifies the most vulnerable sites, such as administrative buildings, economical areas, schools, and churches. We see that the penetration of tsunami inundation for this PMT is very significant in Cap Haitien and that, in view of the large flow velocities in areas close to the shore, many critical buildings and facilities would be severely damaged or even completely destroyed, particularly considering that they would have already been weakened or partially damaged by the earthquake.

Such maps can provide a basis for establishing preliminary crisis management plans, such as evacuation routes, and evacuation areas. More detailed results regarding these aspects, with additional flood mapping, vulnerability assessment, and crisis management plans, will be presented and discussed in a future publication.

4 Conclusions

In this work, we reported on a comprehensive coastal tsunami hazard assessment study along the North Shore of Hispaniola (NSOH), in the Republic of Haiti and the Dominican Republic, from far-field, local, and near-field sources (essentially seismic, with one case of volcanic flank collapse in the Canary Islands). Simulations of coastal tsunami impact were performed by one-way coupling with the long-wave models FUNWAVE-TVD and TELEMAC, in a series of nested grids down to a 205-m resolution in the former model, along the entire coast, and down to a 12–30-m resolution in the latter model, around two selected critical sites: Cap Haiti, Haiti and Puerto Plata, Dominican Republic.

Results first provide a synoptic view of tsunami coastal impact on the NSOH where we see that, among the far-field/local sources, the Cumbre Vieja flank collapse (CVV) causes by far the largest impact, with up to 20-m runup at the critical sites. It should be pointed out that this was obtained using the most extreme CVV scenario with a 450 km³ volume failing at once, which may be too pessimistic; using Abadie et al.'s (2012) so-called expected extreme collapse scenario, with an 80 km³ volume, Tehranirad et al. (2015) found about one-third the inundation of the extreme scenario along the USEC, which could be expected to occur also for the NSOH. The M_w 9 Puerto Rico seismic source (PRT) causes the next largest impact among the far-field/local sources, with up to 4-m runup at the sites and the impact from a M_w 9 earthquake in the Azores convergence zone (LSB) can be considered as negligible in view of those (with less than 1-m runup). A CVV-induced tsunami would reach the NSOH after 6.5 h, while a PRT tsunami would start impacting it after 30 min. This short propagation time, coupled to a much shorter return period (a few hundred years compared to over 100,000 years for CVV), make PRT the most hazardous of the far-field/local sources (in terms of probability of a given impact). In the near-field, a M_w 8.7 earthquake in the North Hispaniola Thrust Fault (NHTF) subduction zone, whose return period would likely be longer than that of PRT, dominates tsunami coastal hazard along the NSOH, with up to 12-m runup at the critical sites combined with propagation times of minutes that would afford very little warning time. Based on impact and travel time, despite a longer return period, the latter event can be considered as the Probable Maximum Tsunami for the NSOH. Accordingly, this NHTF-based scenario was selected as one of two scenarios to serve as a basis for the “CARIBE WAVE 2016” tsunami exercise, organized under the framework of the CARIBE EWS (IOC 2015).

Based on these results, fine-grid simulations were performed with TELEMAC at the two critical sites only for the CVV, PRT and NHTF sources. Examples of TELEMAC results are provided for NHTF, in terms of maximum flow depth and current velocity, which

indicate a high vulnerability of Cap Haitien and its critical infrastructures to this event. The detailed maps produced in this work can be used to draw evacuation plans and prepare for crisis management. More details in this respect will be reported in a future publication.

It should be pointed out that no tsunamis generated by SMFs were considered in the present work, while there is evidence (both in the magnitude and focusing of the generated tsunami and in the geological record) that significant SMFs may have been triggered by historical events such as the 1842 earthquake, which likely struck in the SF. SMF tsunamis are also known to have occurred around Hispaniola, such as in 1918 in the Mona Passage between Hispaniola and Puerto Rico (López-Venegas et al. 2015). Hence, future work should not only perform detailed coastal modeling for additional critical sites, but also site, parameterize, and model relevant future SMFs that could contribute to tsunami hazard along the NSOH.

Acknowledgments This research was supported by UNESCO funding. The authors are solely responsible for the results presented in this paper. The two lead authors also acknowledge support from the US NOAA National Tsunami Hazard Mitigation Program (NTHMP) for the background work on the far-field tsunami sources.

References

- Abadie S, Morichon D, Grilli ST, Glockner S (2010) Numerical simulation of waves generated by landslides using a multiple-fluid Navier–Stokes model. *Coast Eng* 57:779–794. doi:10.1016/j.coastaleng.2010.03.003
- Abadie S, Harris JC, Grilli ST, Fabre R (2012) Numerical modeling of tsunami waves generated by the flank collapse of the Cumbre Vieja Volcano (La Palma, Canary Islands): tsunami source and near field effects. *J Geophys Res* 117:C05030. doi:10.1029/2011JC007646
- Baptista MA, Heitor S, Miranda JM, Miranda PMA, Mendes Victor L (1998a) The 1755 Lisbon earthquake; evaluation of the tsunami parameters. *J Geodyn* 25:143–157
- Baptista MA, Heitor S, Miranda JM, Miranda PMA, Mendes Victor L (1998b) Constraints on the source of the 1755 Lisbon tsunami inferred from numerical modeling of historical data on the source of the 1755 Lisbon tsunami. *J Geodyn* 25:159–174
- Baptista MA, Miranda JM, Chierici F, Zitellini N (2003) New study of the 1755 earthquake source based on multi-channel seismic survey data and tsunami modeling. *Nat Hazards Earth Syst Sci* 3:333–340
- Barkan R, ten Brick US, Lin J (2009) Far field tsunami simulations of the 1755 Lisbon earthquake: implication for tsunami hazard to the US East Coast and the Caribbean. *Mar Geol* 264:109–122
- Benford B, DeMets C, Calais E (2012) GPS estimates of microplate motions, northern Caribbean: evidence for a Hispaniola microplate and implications for earthquake hazard. *Geophys J Int* 191(2):481–490. doi:10.1111/j.1365-246X.2012.05662.x
- Calais E, Mercier de Lepinay B (1995) Strike-slip tectonic processes in the northern Caribbean between Cuba and Hispaniola (Windward Passage). *Mar Geophys Res* 17(1):63–95
- Calais E, Freed A, Mattioli G, Amelung F, Jónsson S, Jansma P, Hong S-H, Dixon T, Prépetit C, Momplaisir R (2010) Transpressional rupture of an unmapped fault during the 2010 Haiti earthquake. *Nat Geosci* 3(11):749–799. doi:10.1038/NGEO992
- Corral Á (2006) Dependence of earthquake recurrence times and independence of magnitudes on seismicity history. *Tectonophysics* 424(3):177–193. doi:10.1016/j.tecto.2006.03.035
- Day SJ, Watts P, Grilli ST, Kirby JT (2005) Mechanical models of the 1975 Kalapana, Hawaii earthquake and tsunami. *Mar Geol* 215:59–92. doi:10.1016/j.margeo.2004.11.008
- Dolan JE, Wald DJ (1998) The 1943–1953 north-central Caribbean earthquakes: active tectonic setting, seismic hazards, and implications for Caribbean-North America plate motions. *Special papers-geological Society of America*, 143–169
- Fritz HM, Hillaire JV, Molire E, Wei Y, Mohammed F (2013) Twin tsunamis triggered by the 12 January 2010 Haiti earthquake. *Pure Appl Geophys* 170(9–10):1463–1474. doi:10.1007/s00024-012-0479-3
- Gailler A, Calais E, Hébert H, Roy C, Okal E (2015) Tsunami scenarios and hazard assessment along the northern coast of Haiti. *Geophys J Int* 203(3):2287–2302. doi:10.1093/gji/ggv428

- Geist E, Lynett P, Chaytor J (2009) Hydrodynamic modeling of tsunamis from the Currituck landslide. *Mar Geol* 264:41–52. doi:[10.1016/j.margeo.2008.09.005](https://doi.org/10.1016/j.margeo.2008.09.005)
- Gica E, Spillane MC, Titov VV, Chamberlin CD, Newman J (2008) Development of the forecast propagation database for NOAA's Short-term inundation forecast for tsunamis. NOAA Tech. Memo. OAR PMEL-139
- Glimsdal S, Pedersen GK, Harbitz CB, Løvholt F (2013) Dispersion of tsunamis: Does it really matter? *Nat Hazards Earth Syst Sci* 13:1507–1526. doi:[10.5194/nhess-13-1507-2013](https://doi.org/10.5194/nhess-13-1507-2013)
- Grilli AR, Grilli ST (2013a) Modeling of tsunami generation, propagation and regional impact along the US East Coast from the Azores Convergence Zone. Research report no. CACR-13-04, 20 pps. <http://personal.egr.uri.edu/grilli/grilli-grilli-cacr-13-04>
- Grilli AR, Grilli ST (2013b) Modeling of tsunami generation, propagation and regional impact along the upper US East coast from the Puerto Rico trench. Research Report no. CACR-13-02, 18 pps. <http://personal.egr.uri.edu/grilli/grilli-grilli-cacr-13-02>
- Grilli ST, Ioualalen M, Asavanant J, Shi F, Kirby JT, Watts P (2007) Source constraints and model simulation of the December 26, 2004 Indian Ocean tsunami. *J Waterw Port Coast Ocean Eng* 33:414–428
- Grilli ST, Dubosq S, Pophet N, Pérignon Y, Kirby JT, Shi F (2010) Numerical simulation and first-order hazard analysis of large co-seismic tsunamis generated in the Puerto Rico trench: near-field impact on the North shore of Puerto Rico and far-field impact on the US East Coast. *Nat Hazards Earth Syst Sci* 10:2109–2125. doi:[10.5194/nhess-2109-2010](https://doi.org/10.5194/nhess-2109-2010)
- Grilli ST, Harris JC, Tajalibakhsh T, Masterlark TL, Kyriakopoulos C, Kirby JT, Shi F (2013c) Numerical simulation of the 2011 Tohoku tsunami based on a new transient FEM co-seismic source: comparison to far- and near-field observations. *Pure Appl Geophys* 170:1333–1359. doi:[10.1007/s00024-012-0528-y](https://doi.org/10.1007/s00024-012-0528-y)
- Grilli ST, O'Reilly C, Harris JC, Tajalli-Bakhsh T, Tehranirad B, Banihashemi S, Kirby JT, Baxter CDP, Eggeling T, Ma G, Shi F (2015a) Modeling of SMF tsunami hazard along the upper US East Coast: detailed impact around Ocean City, MD. *Nat Hazards* 76(2):705–746. doi:[10.1007/s11069-014-1522-8](https://doi.org/10.1007/s11069-014-1522-8)
- Grilli ST, Grilli AR, Tehranirad B, Kirby JT (2015b) Modeling tsunami sources and their propagation in the Atlantic Ocean for coastal tsunami hazard assessment and inundation mapping along the US East Coast. In: Proceedings of the 2015 COPRI Solutions to Coastal Disasters Conference, (Boston, USA, September 9–11, 2015), American Soc. Civil Eng., 12 pps. (in press)
- Hayes GP, Briggs RW, Sladen A, Fielding EJ, Prentice C, Hudnut K, Simons M (2010) Complex rupture during the 12 January 2010 Haiti earthquake. *Nat Geosci* 3(11):800–805. doi:[10.1038/NNGEO977](https://doi.org/10.1038/NNGEO977)
- Harbitz CB, Glimsdal S, Bazin S, Zamora N, Lovholt F, Bungum H, Smebye H, Gauer P, Kjekstad O (2012) Tsunami hazard in the Caribbean: regional exposure derived from credible worst case scenarios. *Cont Shelf Res* 8:1–23. doi:[10.1016/j.csr.2012.02.006](https://doi.org/10.1016/j.csr.2012.02.006)
- Hervouet JM (2007) Hydrodynamics of free surface flows: modeling with the finite element method. Wiley, Colorado, p 360
- Hornbach MJ, Braudy N, Briggs RW, Cormier MH, Davis MB, Diebold JB, Johnson III HE (2010) High tsunami frequency as a result of combined strike-slip faulting and coastal landslides. *Nature Geoscience*. doi:[10.1038/ngeo975](https://doi.org/10.1038/ngeo975)
- IOC (Intergovernmental Oceanographic Commission) (2013) Exercise Caribe Wave/Lantex 14. A Caribbean and Northwestern Atlantic Tsunami Warning Exercise, 26 March 2014. Volume 1: Participant Handbook, IOC Technical Series, 109 vol. 1. Paris: UNESCO
- IOC (Intergovernmental Oceanographic Commission) (2015) Intergovernmental Coordination Group for the Tsunami and other Coastal Hazards Warning System for the Caribbean and Adjacent Regions (ICG/CARIBE-EWS). Tenth Session, Paris: UNESCO
- López-Venegas AM, Horrillo J, Pampell-Manis A, Huérfano V, Mercado A (2015) Advanced tsunami numerical simulations and energy considerations by use of 3D2D coupled models: the October 11, 1918 Mona passage tsunami. *Pure Appl Geophys* 172(6):1679–1698. doi:[10.1007/s00024-014-0988-3](https://doi.org/10.1007/s00024-014-0988-3)
- Ioualalen M, Asavanant J, Kaewbanjak N, Grilli ST, Kirby JT, Watts P (2007) Modeling the 26th December 2004 Indian Ocean tsunami: case study of impact in Thailand. *J Geophys Res* 112:C07024. doi:[10.1029/2006JC003850](https://doi.org/10.1029/2006JC003850)
- Kirby JT, Shi F, Tehranirad B, Harris JC, Grilli ST (2013) Dispersive tsunami waves in the ocean: model equations and sensitivity to dispersion and Coriolis effects. *Ocean Modell* 62:39–55. doi:[10.1016/j.ocemod.2012.11.009](https://doi.org/10.1016/j.ocemod.2012.11.009)
- Knight B (2006) Model predictions of Gulf and Atlantic coast tsunami impacts from a distribution of sources. *Sci Tsunami Hazards* 24(5):304–312
- Lander JF (1997) Caribbean tsunamis: an initial history. *Nat Hazards* 3:1–18
- Madsen PA, Fuhrman DR, Schaffer HA (2008) On the solitary wave paradigm for tsunamis. *J Geophys Res* 113:C12012

- McMurtry GM, Tappin DR, Sedwick PN, Wilkinson I, Fietzke J, Sellwood B (2007) Elevated marine deposits in Bermuda record a late Quaternary megatsunami. *Sediment Geol* 200(3–4):155–165. doi:[10.1016/j.sedgeo.2006.10.009](https://doi.org/10.1016/j.sedgeo.2006.10.009)
- Okada Y (1985) Surface deformation due to shear and tensile faults in a half space. *Bull Seismol Soc Am* 75(4):1135–1154
- Ramalho RS, Winckler G, Madeira J, Helffrich GR, Hiplito A, Quartau R, Adena K, Schaefer JM (2015) Hazard potential of volcanic flank collapses raised by new megatsunami evidence. *Sci Adv* 1(9):e1500456
- Shi F, Kirby JT, Harris JC, Geiman JD, Grilli ST (2012) A high-order adaptive time-stepping TVD solver for Boussinesq modeling of breaking waves and coastal inundation. *Ocean Modell* 43–44:36–51. doi:[10.1016/j.ocemod.2011.12.004](https://doi.org/10.1016/j.ocemod.2011.12.004)
- Shimozono T, Cui H, Pietrzak JD, Fritz HM, Okayasu A, Hooper AJ (2014) Short wave amplification and extreme runup by the 2011 Tohoku tsunami. *Pure Appl Geophys* 171(12):3217–3228. doi:[10.1007/s00024-014-0803-1](https://doi.org/10.1007/s00024-014-0803-1)
- Tappin DR, Watts P, Grilli ST (2008) The Papua New Guinea tsunami of 1998: anatomy of a catastrophic event. *Nat Hazards Earth Syst Sci* 8:243–266
- Tappin DR, Grilli ST, Harris JC, Geller RJ, Masterlark T, Kirby JT, Shi F, Ma G, Thingbaijam KKS, Maig PM (2014) Did a submarine landslide contribute to the 2011 Tohoku tsunami? *Mar Geol* 357:344–361. doi:[10.1016/j.margeo.2014.09.043](https://doi.org/10.1016/j.margeo.2014.09.043)
- Tehraniad B, Shi F, Kirby JT, Harris JC, Grilli ST (2011) Tsunami benchmark results for fully nonlinear Boussinesq wave model FUNWAVE-TVD, Version 1.0. Technical report, No. CACR-11-02, Center for Applied Coastal Research, University of Delaware
- Tehraniad B, Harris JC, Grilli AR, Grilli ST, Abadie S, Kirby JT, Shi F (2015) Far-field tsunami hazard in the north Atlantic basin from large scale flank collapses of the Cumbre Vieja volcano, La Palma. *Pure Appl Geophys* 172(12):3,589–3,616. doi:[10.1007/s00024-015-1135-5](https://doi.org/10.1007/s00024-015-1135-5)
- ten Brink U, Twichell D, Geist E, Chaytor J, Locat J, Lee H, Buczkowski B, Barkan R, Solow A, Andrews B, Parsons T, Lynett P, Lin J, Sansoucy M (2008) Evaluation of tsunami sources with the potential to impact the U.S. Atlantic and Gulf coasts. USGS Administrative report to the US Nuclear Regulatory Commission, p 300
- ten Brink US, Bakun WH, Flores CH (2011) Historical perspective on seismic hazard to Hispaniola and the northeast Caribbean region. *J Geophys Res (Solid Earth)* 106:B12
- UNESCO (2013) Earthquake and tsunami hazard in Northern Haiti: historical events and potential sources. Meeting of experts (Port-au-Prince, Haiti 10–11 July 2013). Workshop report no. 255, p 32
- von Hillebrandt-Andrade C (2013) Minimizing Caribbean tsunami risk. *Science* 341:966–968
- Ward SN, Day S (2001) Cumbre Vieja Volcano—Potential collapse and tsunami at La Palma, Canary Islands. *J Geophys Res Lett* 28:3397–3400. doi:[10.1029/2001GL013110](https://doi.org/10.1029/2001GL013110)
- Watts P, Grilli ST, Kirby JT, Fryer GJ, Tappin DR (2003) Landslide tsunami case studies using a Boussinesq model and a fully nonlinear tsunami generation model. *Nat Hazards Earth Syst Sci* 3:391–402
- Wei G, Kirby JT, Grilli ST, Subramanya R (1995) A fully nonlinear Boussinesq model for free surface waves. Part I: highly nonlinear unsteady waves. *J Fluid Mech* 294:71–92
- Wynn RB, Masson DG (2003) Canary Island landslides and tsunami generation: Can we use turbidite deposits to interpret landslide processes? In: Locat J, Mienert J (eds) *Submarine mass movements and their consequences*. Kluwer Acad., Dordrecht, pp 325–332